

1 **Modification and validation of a commercial dynamic chamber for reactive**
2 **nitrogen and greenhouse gas flux measurements**

3 Moxy Shah¹, Kifle Z. Aregahegn¹, Danial Nodeh-Farahani¹, Leigh R. Crilley^{1,‡}, Tasnia Hasan¹,
4 Yashar Ebrahimi-Iranpour¹, Fahim Sarker¹, Nick Nickerson², Chance Creelman², Sarah Ellis²,
5 Alexander Moravek^{1,§}, Trevor C. VandenBoer^{1,*}

6
7 ¹ Department of Chemistry, York University, Toronto, Ontario, Canada

8 ² Eosense Inc., Dartmouth, Nova Scotia, Canada

9 [‡] Now at: Atmospheric Services, WSP Australia, Brisbane, QLD, Australia

10 [§] Now at: German Environment Agency, Department of Air Quality, Dessau-Rosslau, Germany

11

12 *Communicating author: tvandenb@yorku.ca

13

14

15 **Abstract**

16 Reactive nitrogen compounds (NO, NO₂, HONO, NH₃ and others; N_r) play important roles in
17 atmospheric processes, and their cascading impacts throughout the Earth system have adverse
18 effects on both the environment and human health. The fluxes of these gases at the surface-
19 atmosphere interface have been studied in isolation or smaller subsets, but simultaneous fluxes of
20 all N_r alongside standard greenhouse gases (GHGs) have not been reported. Here, a dual-dynamic
21 chamber system was developed for N_r by modifying a commercially available system for GHG
22 fluxes for use with destructive analyzers, including a reference chamber to account for chemical
23 challenges. The resulting platform makes the measurement of N_r and, by extension other reactive
24 gases, more widely accessible to the scientific community, as custom chambers do not need to be
25 fabricated.

26

27 System modifications to passivate surfaces reduced an initial 36% loss of NO₂ due to
28 transformations below analyzer detection limits (~10%) for relevant atmospheric conditions. The
29 modified 72 L chamber response times did not change for GHGs or NO at a flow rate of 2 L min⁻¹
30 ($\tau = 37\text{-}39$ min versus 36 min). The modifications improved the transfer of NO₂, HONO, and

31 NH_3 by up to 2 min, but substantial surface interactions for NH_3 remain. A surface interaction term
32 was characterized for these gases to obtain accurate field fluxes via a mass balance framework.

33
34 Proof-of-concept measurements of N_r fluxes from agricultural soil samples under controlled lab
35 conditions as a function of soil water content were able to quantify emissions of NO , NO_2 , HONO ,
36 NH_3 , and N_2O simultaneously, without amendment and when subject to N_r fertilization.
37 Unfertilized soils showed variability in NO_2 and HONO emissions when soil structure was
38 minimally disturbed, consistent with in-situ field measurements from others. These oppose
39 maximum potential fluxes in prior lab soil manipulations, particularly for HONO relative to NO .
40 Last, N_r field fluxes were quantified with the dual-chamber system on an in-use agricultural soil,
41 including a urea-based fertilizer perturbation to stimulate microbial and chemical transformation
42 and transfer N_r to the atmosphere. Good agreement with other field flux techniques was found.
43 The mass balance terms within the dual-chamber approach are fully inspected from the pilot
44 deployment in the field, along with an error analysis, to aid in the uptake of this approach by the
45 community.

46

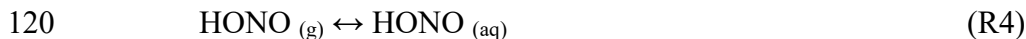
47 1 Introduction

48 Earth's biogeochemical nitrogen (N) cycle is essential for sustaining life through the production
49 of nucleic acids, proteins, and other vital biomolecules (Lehnert et al., 2021). The carbon cycle
50 receives much focus due to the climate impacts greenhouse gases (GHGs) like carbon dioxide
51 (CO_2) and methane (CH_4), yet the N cycle is intertwined (Schlesinger, 2020). At the interface of
52 these cycles and the Earth's surface, reactive nitrogen (N_r) species exchanged between ecosystems
53 and the atmosphere have therefore become an area of emerging interest (Lehnert et al., 2021; Wu
54 et al., 2020). Atmospheric N_r species such as nitric oxide (NO) and nitrogen dioxide (NO_2) –
55 collectively referred to as NO_x – ammonia (NH_3), and nitrous acid (HONO) can experience
56 surface-atmosphere exchange, impacting local air or water quality, ecosystem processes, and
57 biodiversity (Lehnert et al., 2021; Richardson et al., 2023; Wu et al., 2020). Meanwhile, the non-
58 reactive nitrous oxide (N_2O) has climate impacts due to its ~120-year lifetime (IPCC, 2023).

59 Reactive nitrogen gases (NO, NO₂, HONO, and NH₃; N_r) play important roles in atmospheric
60 processes, contributing to the formation of pollutants like ozone (O₃) and secondary organic
61 aerosols (SOA). The exchange of N_r between the Earth's surface and the atmosphere involves
62 production and loss processes driven by both natural and human activities. They are removed
63 through wet and dry deposition, and their abundance reflects the net outcome relative to emissions
64 (Delaria & Cohen, 2023). At the land surface, N_r is released into the atmosphere by microbial
65 nitrogen cycling, agricultural activities, wildfires, or fossil fuel combustion (Benedict et al., 2017;
66 Mosier, 2008; Yang et al., 2024). Studying N_r at the surface-atmosphere interface with high time
67 resolution and chemical speciation remains a challenge due to its high spatial and temporal
68 variability driven by factors like climate, vegetation cover, and soil/surface properties (Ludwig et
69 al., 2001). For example, vertically resolved HONO production observed at the ground surface
70 demonstrated how it plays a major role in the unexplained daytime HONO source and its impact
71 on daytime OH (VandenBoer et al., 2013, 2015; Young et al., 2012). Such observations pose a
72 challenge because suitable high time resolution equipment is expensive, preventing the interplay
73 between emission and deposition for all N_r species from being concurrently studied. As a result,
74 no systems are sufficiently accessible to the scientific community to be deployed widely across
75 different global landscapes, particularly soils.

76 Soils have a dual function as both a source and a sink of N_r species. Soil-atmosphere exchange of
77 N_r is thought to be governed by atmospheric abundance and/or soil microbial processes such as
78 nitrification and denitrification, with factors like pH, moisture, organic matter, and nitrogen
79 availability regulating flux directionality (Mosier, 2008; Purchase et al., 2023; Stepniewski et al.,
80 2015). Microbial processes have been demonstrated to drive the formation and release of N_r
81 species like NO, NH₃ and N₂O from soils, and have assertions with respect to HONO (Butterbach-
82 Bahl & Dannenmann, 2011; Kool et al., 2010; Mushinski et al., 2019; Oswald et al., 2013; Su et
83 al., 2011). Understanding the exchange of all N_r gases is essential for unravelling the complex
84 interactions between the nitrogen and carbon cycles and their broader environmental impacts from
85 an unprecedented imbalance in the global nitrogen cycle (Richardson et al., 2023, Fowler et al.,
86 2013).

87 To quantify N_r exchange for a few explicit species near the ground surface, various flux
88 measurement techniques have been employed. Quantifying fluxes of atmospheric gases has been



123 These processes in/on the chamber can introduce uncertainty in flux measurements. Characterizing
124 and accounting for chemistry and surface effects in chamber-based flux methods are therefore
125 necessary. Static chamber systems typically determine the flux from the change in headspace
126 concentration after closing the cover. Dynamic chamber systems have traditionally used a
127 controlled flow of ambient air through the headspace to retrieve the flux from a concentration
128 difference between the chamber inlet and outlet. The dynamic chamber flux method has measured
129 challenging gases like biogenic volatile organic compounds, such as monoterpenes and isoprene,
130 from vegetation and farmland (Kolari et al., 2012; Mochizuki et al., 2018, Pugliese et al. 2023),
131 NH_3 volatilization from cattle manure (Becciolini et al., 2024), N_2O and NO_x from turfgrass
132 (Maggiotto et al., 2000), and NO_x from grasslands (Pape et al., 2009; Plake et al., 2015). Scharko
133 et al. (2015) used sealed chambers, while Tang et al. (2019) used dynamic, to highlight the hotspot
134 potential for both HONO and NO_x fluxes from agricultural soils [Click or tap here to enter text.](#)
135 These are of high interest due to their impacts on atmospheric chemistry from local to regional
136 scales. The complex biological and chemical controls on nitrite (NO_2^-) production and loss in soils,
137 coupled with soil properties facilitating gas exchange of HONO, has led to intense interest and
138 debate around discerning the fundamental controls on its surface-atmosphere exchange (R4, R5)
139 (Barney & Finlayson-Pitts, 2000; Huang et al., 2002; Kamboures et al., 2008; Meusel et al., 2018;
140 Mushinski et al., 2019; Purchase et al., 2023; Song et al., 2023; Sörgel et al., 2015; Wang et al.,
141 2021). The same is true for direct emissions of NO_2 from soils, where evidence remains limited
142 and the uncertainty is high (Huber et al., 2024; Zörner et al., 2016). For example, Gong et al. (2025)
143 estimate that fertilizer-induced soil NO_x emissions contribute 0.84–2.20 Tg N yr⁻¹ globally, with
144 uncertainty partly due to a lack of NO_2 measurements. Their modelling suggests this
145 underestimates summertime ozone enhancements by 0.3–3.3 ppbv in agricultural hotspot regions,
146 and has been implemented further in other atmospheric models (Ha et al., 2023; Tian et al., 2024).
147 This N_r exchange in agricultural regions from excessive nitrogen inputs are prime targets for

148 chamber methodologies, as they amplify emissions of all N_r species (Degaspari et al., 2020; Huber
149 et al., 2020; Manco et al., 2025). These issues highlight the need for more direct soil NO₂ and
150 HONO measurements, as well as simultaneous constraints on the entire N_r suite being exchanged
151 from soils.

152 Automated dynamic chambers deployed in situ for field observations and performing controlled
153 experiments would provide a platform for capturing the magnitude, direction, and temporal
154 variability of N_r species or physical variables via the headspace gas or soil amendments while
155 retaining soils in an intact state (Aneja et al., 2006). Thus, establishing an accessible dynamic
156 chamber method for N_r flux measurements is desirable. However, such a platform needs to
157 undergo extensive validation to reduce flux bias from challenging N_r species such as NH₃. This
158 important and necessary first step will allow a wider global study of surface-atmosphere N_r
159 exchange processes. One of the best existing examples to date of automated dynamic chamber
160 design for N_r measurements, is the custom-built system from Pape et al. (2009) who measured NO,
161 NO₂, and O₃ to deploy an unattended array of six samplers with destructive gas analyzers. In their
162 system, a reference chamber was used to characterize system surface effects, while using a large
163 volume flow through the headspace during chamber closure periods to quantify fluxes on the
164 assumption that ambient levels were not dramatically changing (e.g. due to nearby point sources).
165 This work synthesized many advantages from similar designs to study soil- and plant-atmosphere
166 interactions, but the technique remains accessible only to researchers with in-house engineering
167 design and fabrication facilities. In the intervening years, dynamic chambers for GHG fluxes have
168 become widely commercialized to improve measurement capacity compared to static chamber
169 determinations and to make flux observations more accessible compared to conducting eddy
170 covariance measurements.

171 Here, we bridge several gaps to link the atmospheric GHG and N_r flux communities to yield a
172 dynamic flux system for CO₂, CH₄, N₂O, NO, NO₂, HONO, and NH₃. First, we modify commercial
173 dynamic chambers with large volume (72 L) and footprint (0.21 m²) originally designed for trace
174 GHG flux measurements to make them suitable for quantifying the most prevalent N_r gas exchange
175 fluxes at surface-atmosphere interfaces, meaning the apparatus is more widely available to the
176 atmospheric community. Next, we implement surface and hardware modifications to adapt the
177 commercial chambers to minimize gas adsorption and transformations, so that more reactive gases

178 such as HONO and NH₃ can be added to the N_r flux analyte suite. We systematically characterized
179 the transfer of both GHGs and N_r species by calculating fill and empty rates, transformed to time
180 constants, to identify any surface interactions and/or transformations on the chamber surfaces. We
181 then applied our modified commercial dynamic chambers to make flux measurements by
182 equipping them with destructive gas analyzers for HONO and NO_x and a cavity ring-down
183 spectrometer (Picarro G2509) for NH₃, N₂O, CO₂, and CH₄ in lab experiments, or with a fully
184 automated dual-chamber approach under field conditions through a pilot study with 30 minute
185 closures to obtain a sufficient number of measurements to detect relevant fluxes with standard gas
186 analyzers. Fluxes during the pilot study were assessed by rate of change determinations during
187 closure periods and bias minimized through a mass balance to demonstrate system capabilities for
188 several N_r gases in an agricultural field. This community-accessible approach addresses key needs
189 by allowing more researchers to measure N_r exchange at the surface-atmosphere interface, with
190 the added benefit over past systems to monitor fluxes of all species simultaneously with at least
191 hourly time resolution when using gas analyzers with one-minute measurement frequencies.

192 **2. Materials and methods**

193

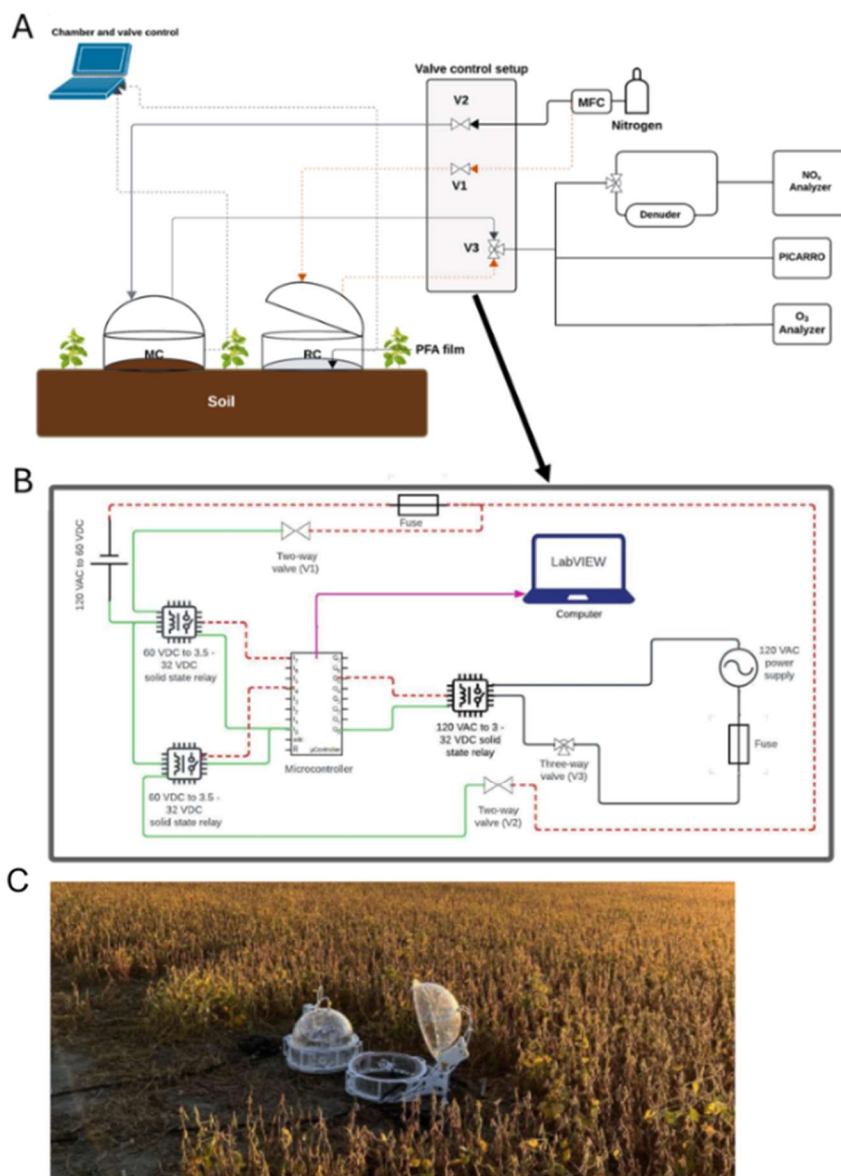
194 **2.1 Dynamic Chambers for Field Fluxes**

195 **2.1.1 Description of custom-modified dual-dynamic chambers fluxes**

196 The dynamic chamber system uses two identical commercially available units (eosAC-LT
197 Eosense, Dartmouth, NS). These are modified and coupled to programmable valves that control
198 sample gases delivered to a suite of instrumentation (Figure 1).

199 The dynamic chambers are constructed with transparent polyacrylate walls and lids, with an
200 internal volume of 0.072 m³ (72 L) and bottom surface area of 0.21 m². When used on soils the
201 chambers are secured with collars and custom-made polytetrafluorethylene (PTFE) rings (Figure
202 S1). A built-in fan ensures uniform distribution of gases inside the chamber. Air temperature is
203 measured inside from the fan arm, pressure is from the control box outside the chamber, and two
204 auxiliary ports, one internal and external, can collect environmental properties such as relative
205 humidity (RH), photosynthetically active radiation (PAR), soil temperature, and/or soil volumetric
206 water content (VWC).

207 For a N_r sampling approach, one chamber is used as the measurement (MC) from an experimental
208 surface while the second is a reference (RC) sealed at the bottom with a $51\ \mu\text{m}$ ($0.002''$) film of
209 perfluoroalkoxy alkane (PFA; McMaster-Carr®, PN: 84955K24). The inert PFA film is held in
210 place between the chamber collar and our custom-made PTFE rings (Figure S1). The RC acts as a
211 negative control for physical interactions and/or associated chemistry of reactive gases on chamber
212 and gas transfer line surfaces. The use of the RC, therefore, is to facilitate the correction of surface-
213 mediated effects, reactions, and reduction of bias when determining quantitative flux values.



214

215 **Figure 1. (A)** Schematic of the dynamic chamber system to measure N_r and GHG fluxes. The
216 components of the system include: the chambers, a dilution gas source (nitrogen (N_2) or zero air
217 (ZA)), solenoid valve control, gas transfer lines, and gas analyzers. Grey lines indicate dilution gas
218 flow from a source (e.g. cylinder) to the measurement chamber (MC) and air sampled from the
219 MC to the analyzers. The dashed orange line represents these same flows relative to the reference
220 chamber (RC). Communication lines from the chambers to a computer for automated control and
221 ancillary sensor data collection using the chamber software (eoslink-AC; blue dotted lines). **(B)**
222 The valve control setup for flow control in the complete dynamic chamber system, illustrating
223 electrical components and lines needed for full automation using LabVIEW. It includes two 24 V
224 DC two-way valves (V1 and V2; red dashed lines for negative electric potential, green for
225 positive), with power supplied by solid-state relays, and a three-way 120 V AC valve (V3; black
226 lines) with a power supply and another solid-state relay. The purple arrow represents the USB data
227 acquisition connection from the microcontroller to a computer running the LabVIEW VI for valve
228 control. **(C)** Field deployment of the dynamic chamber system, where the closed chamber is the
229 reference and the open chamber functions as the measurement chamber.

230

231 The RC component of this system is designed to continuously baseline the physical interactions
232 and chemistry happening on its surfaces both before and after quantifying reactive gas fluxes with
233 the MC. Thus, the measurements are taken every 30 minutes, where one chamber is closed for gas
234 analysis while the other is open to the ambient atmosphere. The sampling time interval was
235 determined based on i) obtaining enough measurements at 1-minute time resolution to perform a
236 reliable accumulation or loss linear regression, and ii) an ability to readily detect the lower limit
237 of the range of field HONO flux values reported in the literature to ensure detection in its
238 application during our pilot field study (see Section 2.7). For the first criterion, this also includes
239 an exclusion of the first and last few measurements (3 to 5) to allow for complete gas replacement
240 between the chamber lines and the analyzers, and disruption of the sealed environment as the
241 chamber cycle alternates, respectively. The resulting accumulated mixing ratios of HONO in the
242 chamber are well above the 1.4 parts per billion (ppbv) mixing ratio detection limit (LOD) of even
243 a modified NO_x analyzer, such that it can be used for measuring HONO (Crilley et al., 2023; Lao
244 et al., 2020; Zhou et al., 2018; Nodeh-Farahani et al., 2021).

245 Headspace recirculation to facilitate analyte mixing ratio accumulation or depletion for non-
246 destructive spectroscopic GHG analysis is a common measurement approach to decrease flux
247 observation times. Reactive nitrogen measurements, in contrast, are typically destructive
248 techniques that change the identity of the target analyte in the act of quantifying its abundance. To
249 interface with such instruments, the sampled air needs to be replaced (Linde Canada Plc, PN: NI

250 LC250-230) to balance the flow demand in a closed chamber. This balance is delicate even when
251 using mass flow controllers (MFCs) on both incoming and outgoing flows, and the best solution
252 we identified is to provide a slight overflow that takes advantage of the chamber design to vent
253 excess pressure through a short length (~15 cm) of 1/8" ID (3.175 mm), 1/4" OD (6.35 mm) tubing
254 that keeps the internal pressure equivalent to ambient. The flow differential between make-up gas
255 and sampling is roughly $400 \text{ cm}^3 \text{ min}^{-1}$. Such a supply of make-up gas was explored across a range
256 of potential flow rates when using destructive gas analyzers (e.g., three instruments each sampling
257 at 1 - 4 standard litres per minute, L min^{-1}) to find that 6 L min^{-1} is the upper limit of flow-through
258 where the chamber pressure is not substantially perturbed from ambient and the chamber lid retains
259 its seal.

260 In the field, a flux measurement cycle begins with closing the RC while the MC is open. At defined
261 intervals, they alternate their open-closed states. Flows of make-up gas to each chamber are
262 modulated with a pair of two-way solenoid valves. When sampling from the RC, one valve (V1;
263 Figure 1) is open to permit make-up gas flow while the other valve (V2) is closed to prevent the
264 flow from being directed to the MC. On the sampling lines, a three-way solenoid valve (V3)
265 alternates to guide flow from whichever is closed to the suite of gas analyzers. All instrument and
266 operational details are provided in Section 2.1.3.

267

268 **2.1.2 Automated controls: system, data collection and processing**

269 The chamber eosLink-AC software (Eosense Inc., Dartmouth, NS) is used to define the duration
270 of chamber opening and closing cycles, and logs chamber temperature, pressure, and auxiliary
271 sensor data associated with a given eosAC-LT chamber. Each chamber requires a 12 V DC power
272 supply connected by USB to a laptop through a weatherproof communication cable, controlling
273 the chamber lid and data transfer.

274 When a chamber cycle begins, a text file is generated and includes measurement time elapsed,
275 chamber lid status, chamber temperature and pressure, and auxiliary sensor data. This data file is
276 updated at least once every 10 seconds, varying between 2-8 second intervals, which we average
277 onto a 1-minute time base to match measurements from the slowest gas analyzers. The solenoid
278 valves are modulated by the electrical circuit shown in Figure 1B. Automation is facilitated by a
279 microcontroller (NI-6509i, National Instruments) programmed with a custom-scripted LabVIEW

280 VI (LabVIEW version 2020). Further design information and full details of this sampling strategy
281 and script can be found in Section S1 of the supporting information, and is available on the GitHub
282 repository alongside our VI (<https://github.com/fjs-vdblelab/fluxchamber.git>).
283

284 **2.1.3 Reactive and greenhouse gas instrumentation for flux measurements**

285 The mixing ratios of NO and NO₂ were measured using a commercially available
286 chemiluminescent NO_x analyzer (EC 9841, American Ecotech, Warren, RI). The calculated LOD
287 determined from sampling dry zero air was 0.84 ppbv, 0.67 ppbv and 1.07 ppbv for NO, NO_x, and
288 NO₂ (or HONO when using the denuder as described below), respectively. The instrument has an
289 operating range of 0 – 20 parts-per-million by volume (ppmv), a sample flow rate of 0.5 L min⁻¹,
290 and reports measurements at a time resolution of 1 minute. To quantify NO₂, it is reduced to NO
291 on a heated molybdenum catalyst (325 °C). To prevent interferences reported by others from
292 atmospherically-relevant acidic species in this system (e.g. HONO, HNO₃, and N₂O₅) the sampled
293 air from the chambers during field experiments was passed through a sodium carbonate (Na₂CO₃)
294 coated annular denuder to reduce bias in the NO₂ measurement, as these species and other
295 components of NO_y (e.g. peroxyacetyl nitrate; PAN) may also be reduced to NO (Villena et al.,
296 2012). The Na₂CO₃ denuder was prepared according to the EPA Compendium Method IO-4.2
297 (Winberry Jr et al, EPA, 1999) to remove atmospheric acids by reactive uptake to the basic coating.
298 As part of our controlled laboratory and pilot field study experiments, this denuder was also used
299 to selectively measure HONO by scrubbing this target gas for a specified period, but would include
300 the other known interferences. If this term is depositing, it could include the other NO_y detected
301 by the same conversion mechanism, but if emitting we expect it to be dominated by HONO.
302 Ideally, a platform like time-of-flight chemical ionization mass spectrometry (ToF-CIMS) would
303 be used for disambiguation but was not available at this time.

304
305 A commercial O₃ analyzer (Serinus 10, American Ecotech, Warren, RI) was used to measure
306 mixing ratios, quantify O₃ loss to surfaces, and constrain the reaction of O₃ with NO to form NO₂
307 in the pilot study sampling. This analyzer employs a non-dispersive UV absorption cell to quantify
308 O₃ in the sampled air. The calculated LOD from sampling zero air is 0.95 ppbv at 1 minute time

309 resolution, with an operating range of 0 to 20 ppmv and a sampling flow rate of 0.5 L min⁻¹. Quality
310 control procedures for the NO_x and O₃ instruments can be found in Section S2.

311 The mixing ratios of the GHGs N₂O, CH₄, CO₂, H₂O, and NH₃ sampled from the automated
312 chamber system were measured using a Picarro G2509 which uses cavity ring down spectroscopy
313 (CRDS). The analyzer has a time response of ~ 8 seconds for N₂O, CH₄, CO₂, H₂O and < 2 min
314 for NH₃. The Picarro G2509 was used for the lab experiments and the pilot field study. The
315 customized version of the instrument sampled at ~0.23 L min⁻¹ and was equipped with an inlet
316 filter. To minimize adsorption and chemical interactions of NH₃ on instrument surfaces, stainless
317 steel gas handling components, including the inlet bulkhead, were replaced with PFA counterparts.
318 The instrument cavity material was treated with a SilcoNert® coating by the manufacturer. We
319 did not observe changes in its performance for the measured gases when operated according to the
320 manufacturer guidelines. The Picarro G2509 analyzer spectroscopic mixing ratio determination
321 means a full span calibration is not a regular necessity. Despite this, we validated its calibration
322 and performed quality control checks in the lab to ensure the accuracy and stability of the analyzer
323 for all aspects of this work (Section S2).

324

325 **2.2 Chamber modifications to minimize NO₂ reactions on chamber surfaces**

326 To transfer reactive gases through these chambers, interactions with surfaces need to be limited at
327 all points of potential adsorptive or reactive losses. The custom-made base plate (Figure S1) was
328 used to assess gas interactions on the commercial chamber surfaces. and identification of parts for
329 replacement. First, the gas inlet and outlet push-to-connect fittings in the original configuration
330 have plastic grips, with an internal component made of brass, which is informally known in the
331 atmospheric chemistry community to have strong interactions with nitrogen oxides. These were
332 replaced with PTFE Swagelok® bulkhead fittings (PN: T-400-1-4; Figure S2). Second, the
333 polyacrylate wall and lid surfaces of the chambers had the 51 μm (0.002”) PFA film applied to the
334 inner surfaces using double-sided tape to retain actinic transparency and PAR transfer to contained
335 plants and surfaces (Figure S2).

336

337

338 2.3 Chamber modification validation using greenhouse and reactive gases

339 Before and after our modifications, we had to ensure that the non-reactive GHG transfer was
340 unchanged in addition to challenge tests for the transfer of N_r gases. It was expected that N_r gases
341 would interact and/or react on chamber surfaces and 15 m of standard sampling tubing that would
342 differ between the unmodified and modified variants. Determining the time constants of fill (E1,
343 E2) and decay (E3, E4) of these interactive and/or reactive gases in the chamber system allowed
344 us to contrast their behaviour against that expected from a modelled theoretical inert trace gas in
345 our system (Figure 2). Equations used to model mass transfer in our chambers were derived from
346 Pape et al. (2009). The resulting accumulation curve was modelled by the theoretical function:

$$347 \quad \mu_{fill}(t) = 1 - e^{-\left(\frac{t}{\tau_{fill}}\right)} \quad (\text{E1})$$

$$348 \quad \tau_{fill} = V/Q_{fill} \quad (\text{E2})$$

349 Where μ_{fill} represents the normalized mixing ratio of the gas in the chamber at the time t (min)
350 after closing of the chamber compared to the maximum mixing ratio within the measurement cycle,
351 τ_{fill} is theoretical accumulation timescale for transfer of an ideal inert gas (min), V is the volume
352 of the chamber (0.072 m^3), and Q_{fill} represents the total experimental flow rate (2 L min^{-1}).
353 Similarly, the theoretical decay curve when emptying the chamber can be obtained, where τ_{emp} is
354 the theoretical decay timescale for gas transfer (min) and Q_{emp} is again the total experimental flow
355 rate (2 L min^{-1}).

$$356 \quad \mu_{emp}(t) = e^{-\left(\frac{t}{\tau_{emp}}\right)} \quad (\text{E3})$$

$$357 \quad \tau_{emp} = \frac{V}{Q_{emp}} \quad (\text{E4})$$

358

359 2.3.1 Instrumentation and materials for control experiments

360 Control experiments for the transmission of GHG and N_r gases were conducted by filling and
361 emptying the chambers with known quantities at mixing ratios relevant to the atmosphere, as well
362 as quantities expected to accumulate during real observations of modest emission fluxes (e.g. from
363 a fertilized farm field). All assessments herein matched: the standard configuration of the chambers
364 with all fittings, 15 m of $\frac{1}{4}$ " O.D. PFA gas transfer tubing, flow rates, valves and gas transfer lines

365 to instrumentation, with line/fitting/valve/instrumentation surfaces included. Details of the
366 generation of gas concentrations can be found in Section S3 of the SI.

367 **2.3.2 Filling and emptying experiments with N_r, O₃, and GHGs**

368 The positive control experiments filled the chambers in both modified and unmodified
369 configurations and time constants were calculated from the measurements. In each filling
370 experiment, the chamber was flushed with pure N₂ from a liquid N₂ dewar (Linde Canada, PN: NI
371 LC250-20) until a stable baseline level of each gas mixing ratio was reached; typically, these were
372 values at the analyzer detection limits. Then, a blend of GHGs or one of the N_r analytes was
373 delivered into the chamber with N₂ dilution flow at a total flow rate of 2 L min⁻¹, which was then
374 sampled at 1.8 L min⁻¹ by the analyzers (Figure S4). The gases were added to the chamber from
375 their respective calibration sources until the observed concentration (C) reached the known value
376 being delivered (C₀), within error. Since different mixing ratios of the gases were added for these
377 control experiments, the use of normalized concentrations was necessary to facilitate data analysis
378 and visualization. Where surface interactions could be identified (e.g. for NH₃), the role of surfaces
379 versus air exchange was explored using double exponential fits (see ES-1 and ES-2 in Section S3)
380 (Crilley et al., 2023; Ellis et al., 2010; Moravek et al., 2019). The gases were emptied back to the
381 initial baseline level before starting the next replicate or a new experiment with a different target
382 gas. Time constants for filling and emptying were determined by fitting the observations in Igor
383 Pro8 (Wavemetrics, Portland, OR, US).

384 Similarly, the Eosense eosMX multiplexer is designed to coordinate chamber flux measurements
385 using eosAC chambers with non-destructive analyzers, such that headspace can be recirculated
386 while the chambers are closed. One of these devices was also characterized following similar
387 modifications. This system is appealing as it has the eosLink-MX software (Eosense, V1.9.07),
388 which is used for communication, scheduling actions, and logging peripheral data from all
389 connected eosAC chambers. It features dedicated chamber tubing inlets and outlets, along with a
390 COMM port supporting up to 12 eosAC chambers. Each chamber channel includes two Swagelok
391 gas fittings for transporting gases to analyzers and for either recirculating, or in the case of N_r
392 measurements, supplying a clean dilution gas to the chamber headspace.

393 To optimize the performance for N_r species, the original stainless-steel (SS) Swagelok fittings and
394 solenoid valves were compared against replacement PFA tube fittings, bulkhead unions
395 (Swagelok, PFA-420-61), and a PTFE 3-way valve (Clippard, NR1-2-12-G2). A 2 L min^{-1} flow
396 of dry zero air containing the target compounds was passed through either the SS valve with SS
397 fittings or the PTFE valve with PFA fittings for 30 minutes each. The flow was measured before
398 and after the valves to ensure the setup was free of leaks. The ratio of the transferred gas amount
399 to the nominal was used to identify impacts of surface interactions on quantitative transmission to
400 downstream gas analyzers. Further details are presented in Sections 2.7 and S4.

401 **2.4 Characterization of NO_2 and O_3 loss on chamber surfaces**

402 All losses of NO_2 in the chamber were characterized by the addition of known NO_2 mixing ratios
403 (5-10 ppbv) to the chamber under relevant relative humidity (RH) conditions (45-85% RH; Figure
404 S5; Section S5). The mixing ratios of NO_2 and RH values selected for these experiments are
405 representative of the ambient atmosphere in urban areas (Toronto North Station, ECCC), where
406 the chamber system was envisioned to be deployed. The experiments were performed
407 progressively and in triplicate with 5 ppbv of NO_2 and 85% RH, starting from the unmodified
408 configuration of the chamber, replacement of fittings, and covering the inner surface with PFA
409 film to quantify their efficacy in minimizing NO_2 loss and/or transformation on chamber surfaces.
410 These were followed by varying NO_2 mixing ratios and RH to characterize the modified system.

411 Quantification of NO_2 and HONO in the air sampled from the chamber can be achieved using the
412 alternating solenoid setup depicted in Figure S5. The sampled air is switched between two channels
413 – one directly to the NO_x analyzer and the other through a Na_2CO_3 -coated denuder – modulated
414 every 5 minutes by a three-way solenoid valve (Fluoroware Galtek 1/4" F-NPT 3-way solenoid
415 valve, 115V, PN: 203-3414-415. Entegris Inc., MN, US). When the sampled air flows directly to
416 the analyzer, the total mixing ratio of NO_2 and acidic NO_y species, like HONO and HNO_3 , is
417 measured and has been termed NO_2^* (Crilley et al., 2023; Lao et al., 2020; Zhou et al., 2019).
418 When the flow is directed through a Na_2CO_3 denuder, it selectively scrubs HONO and HNO_3 ,
419 leaving behind NO_2 (Possanzini et al., 1983). Under the controlled NO_2 composition used in our
420 experiments, it is expected that HONO will be the only acid present in the sampled air, as such
421 experimental systems have been thoroughly characterized by Finlayson-Pitts et al. (2003),⁵ and
422 HNO_3 is retained on the surfaces (R3) (Barney & Finlayson-Pitts, 2000; Huang et al., 2002;

423 Kamboures et al., 2008). As a result, by the differential measurement of mixing ratios recorded in
424 the two channels (E5) every 5 minutes, HONO can be quantified.

$$425 \text{ HONO} = \text{NO}_2^* - \text{NO}_2 \quad (\text{E5})$$

426 To quantify the amount of NO₂ lost to the chamber surface relative to the mixing ratio of NO₂
427 added to the chamber during an experiment, the NO₂ loss fraction (f_{NO₂}) was found to be
428 informative for mass balance between the two processes.

429 Similarly, we tested the modifications and aging of the installed PFA film surfaces on O₃ transfer.
430 It is among the most sensitive/reactive species to transfer through this new system and is expected
431 to drive reactive loss of NO when measuring N_r fluxes. The fraction of O₃ lost to chamber surfaces
432 was quantified from 150-250 ppbv using a clean and unmodified chamber with PTFE bulkhead
433 fittings replacing the push-to-connect brass fittings (Section S5).

434 The fraction of O₃ lost to chamber surfaces was then quantified in duplicate on a modified chamber
435 with the interior chamber surfaces covered by brand new PFA film or one exposed to ambient air
436 for more than two years, with 15 days of continuous use in an agricultural field during our pilot
437 study.

438 **2.5 Proof of concept N_r fluxes from agricultural soils**

439 **2.5.1 Soil sample N_r emissions for lab experiments**

440 Randomized soil samples weighing 4-5 kg were collected into Ziploc[®] bags from an eight-plot
441 grid established at an agricultural field site in Lambton County, ON, Canada (43°09'36.0" N
442 81°55'48.0" W). The samples were used to investigate emissions in the lab with and without the
443 addition of fertilizers. Individual and pooled samples from the field plots were used. Bulk soil
444 samples were prepared for lab-based chamber measurements by removing debris, roots and seeds,
445 followed by oven drying at 35 °C for 24-72 hours on a stainless-steel mesh tray covered with
446 aluminum foil, to prevent alteration of the microbial community from exposure to unrealistic
447 temperature regimes. After drying, samples were stored in Ziploc[®] bags at room temperature until
448 use.

449 Ultrapure water (18 MΩ·cm; Milli-Q[®], Sigma-Aldrich, St, Louis, US) was added to
450 approximately 350 g of a dry soil sample to achieve ~28% volumetric water content (VWC). The
451 soil sample was loaded into the chamber on a foil-lined tray, and the water content was measured

452 using a soil moisture probe inserted fully into the sample (TEROS 11, VWC range for mineral
453 soils: 0.00 – 0.70 m³/m³; accuracy: ± 0.03 m³/m³; resolution: 0.001 m³/m³, METER Group Inc.,
454 WA, USA). Zero air modified to 65% RH was delivered at 3.6 L min⁻¹ to the chamber headspace
455 where the soil was contained. The soil started the drying process from a VWC of approximately
456 25% with the flows held constant for around 4 days or until the VWC reached 15%. The chamber
457 was sealed to conduct the drying cycle while our modified NO_x analyzer and the Picarro G2509
458 measured fluxes. Unamended soil samples and others fertilized with urea (CO(NH₂)₂), ammonium
459 carbonate (AC, (NH₄)₂CO₃), ammonium bicarbonate (ABC, NH₄HCO₃) at rates of 100 kg N ha⁻¹
460 were assessed. A similar experiment was conducted with ammonium nitrate (NH₄NO₃) at the same
461 fertilizer rate using only the modified NO_x analyzer. Soil VWC and headspace RH were recorded
462 using auxiliary sensors within the chamber.

463 **2.5.2 Field deployment of automated dynamic N_r chambers**

464 The RC and MC setup was deployed to make automated N_r flux measurements from the same
465 agricultural field as in the prior section. The observations took place in early September 2022 at
466 the end of a soybean cropping season. A detailed description of the campaign and its results is the
467 subject of a separate work, so we provide a brief overview here. The total measurement period was
468 approximately two weeks in duration to test system performance. Generally, conditions were hot
469 and dry, without precipitation, and the soybeans surrounding the observed soils were undergoing
470 senescence during the measurement period. The chambers were deployed only on the soil, between
471 crop rows, and operated to quantify fluxes as outlined in Section S7. After an initial 7-day period
472 of observing baseline fluxes from the field, an experimental perturbation was conducted to
473 stimulate N_r emissions through the addition of an aqueous urea solution equivalent to 22 kg N ha⁻¹
474 of fertilizer added by broadcast application, followed by washing into the soil by an equivalency
475 of 2.5 cm (1”) of rain depth. The modified NO_x analyzer and the Picarro G2509 were used to
476 measure the N_r and GHG fluxes continuously across both periods.

477 **2.6 Soil flux determination**

478 The flux of a gas is the rate at which it is transferred across an interface (e.g., soil to atmosphere)
479 per unit area per unit time. Gas fluxes are of high interest in agriculture as they give insight into
480 the uptake or emission of N-bearing gases that may alter fertilizing, effects. They are also
481 important for assessing the state of plants or soils at interfaces through metrics like primary

482 productivity, in which case measurement of a GHG like CO₂ provides the insight (Anthony &
 483 Silver, 2024; Li et al., 2016; Okiti et al., 2025). The RC captures environmental fluctuations such
 484 as temperature or pressure change and directly observes the interactions of ambient gases with
 485 surfaces within the sampling setup (i.e. chambers, gas transfer lines, valves, and analyzers), as well
 486 as tracking reactions, allowing for corrections to every net flux (F_{net}) measurement cycle (E6 for
 487 reactive gases and E7 for non-reactive gases, as derived in Section S7).

$$488 \quad F_{\text{net}} = (\lambda) \cdot \left(\frac{V}{A} \left(\frac{\Delta C_m}{\Delta t_m} - \frac{\Delta C_r}{\Delta t_r} \right) + \frac{Q_{\text{out}}}{A} \left(\frac{\int_{t_{1m}}^{t_{2m}} c_m(t) dt}{\Delta t_m} - \frac{\int_{t_{1r}}^{t_{2r}} c_r(t) dt}{\Delta t_r} \right) - \frac{V}{A} \left(\frac{\int_{t_{1m}}^{t_{2m}} R_m(t) dt}{\Delta t_m} - \frac{\int_{t_{1r}}^{t_{2r}} R_r(t) dt}{\Delta t_r} \right) \right)$$

489 **E6**

490 Where V is the volume of the chamber (m³), A is the surface area (m²) enclosed by the chamber
 491 and governing the gas flux; Q_{out} is the volumetric flow rate of air exiting the chamber (m³ s⁻¹);
 492 $c_m(t)$ and $c_r(t)$ are target gas concentrations within the MC and RC (mol m⁻³), respectively; $\frac{\Delta C_m}{\Delta t_m}$
 493 and $\frac{\Delta C_r}{\Delta t_r}$ represent their corresponding rates of change (mol m⁻³ s⁻¹); and F_{net} is the resulting net gas
 494 flux per unit area (mol m⁻² s⁻¹). The terms R_m and R_r denote the instantaneous chemical production
 495 or loss rate expressed in units of mol m⁻³ s⁻¹ for consistency. The dimensionless attenuation factor
 496 λ is required to correct for interactions of reactive gases with surfaces. Such surface interactions,
 497 which are particularly strong for gases like NH₃, significantly reduce the measured rate of
 498 concentration change within the closed chamber (Figure 4). Thus, λ is derived as the ratio between
 499 a theoretical unattenuated gas (i.e. an inert GHG like N₂O) and the target gas concentration from
 500 controlled deliveries integrated over the chamber closure interval as derived in Section S7. This
 501 term has the surface effects from chambers, gas transfer lines, and analyzers embedded by
 502 definition and must be determined empirically for any altered configuration. The attenuation
 503 correction removes bias from surface-induced artifacts in flux estimates, so that more accurate
 504 soil–atmosphere exchange is reported.

$$505 \quad F_{\text{net}} = \lambda \cdot \frac{P_{\text{air}}}{R \cdot T} \cdot \left(\frac{V}{A} \left(\frac{\Delta X_m}{\Delta t_m} - \frac{\Delta X_r}{\Delta t_r} \right) + \frac{Q_{\text{out}}}{A} \left(\frac{\int_{t_{1m}}^{t_{2m}} X_m(t) dt}{\Delta t_m} - \frac{\int_{t_{1r}}^{t_{2r}} X_r(t) dt}{\Delta t_r} \right) \right)$$

506 **E7**

507 For inert gases described by E7, the fluxes can be based on mixing ratios, where X_m and X_r are
508 the gas volumetric mixing ratios (mol X per mol air), P_{air} is the air pressure (Pa), T is the absolute
509 temperature (K), and R is the universal gas constant ($J\ mol^{-1}\ K^{-1}$). By comparing the RC and MC
510 observations, we isolate the effects of specific environmental conditions on N_r (E6) or GHG (E7)
511 exchange fluxes, while accounting for surface effects and chemical transformations in the former.

512 **3 Results**

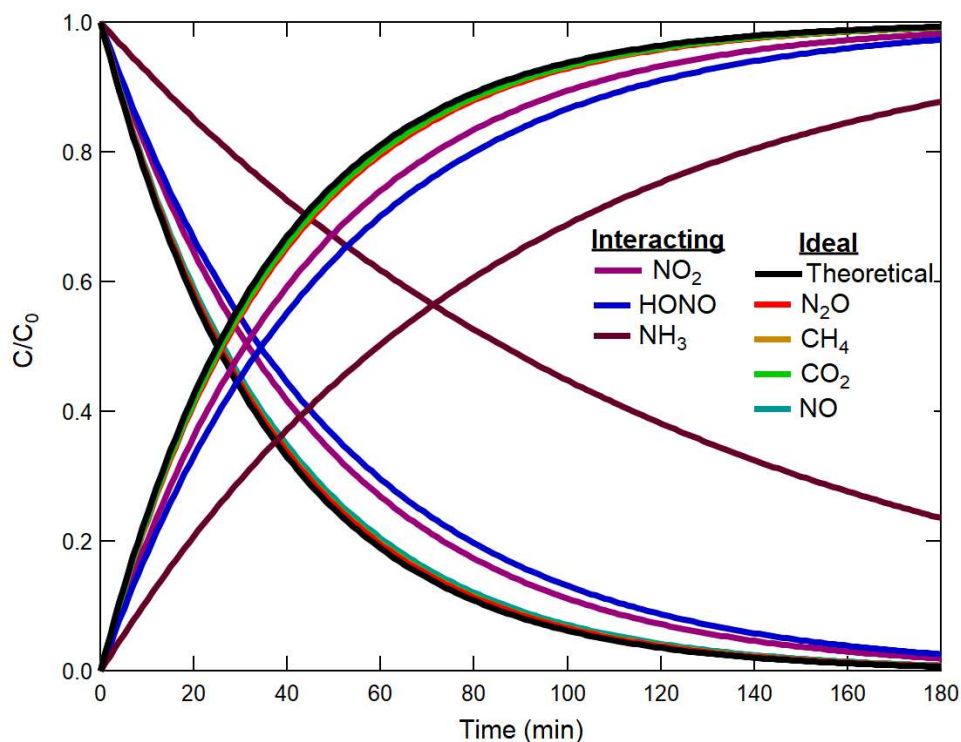
513 **3.1 Determining time constants of reactive nitrogen and GHGs**

514
515 The time constants of both filling and emptying the chambers were calculated using concentrations
516 normalized to their initial values, for each N_r gas and GHG. These were used to quantify gas
517 transfer times through the chambers and to confirm performance relative to theory. Where
518 departures were identified, we quantified the extent of surface interactions for the various target
519 analytes so corrections for determining in situ fluxes could be implemented (Table 1, Figure 2).

520 **3.1.1 Time constants of greenhouse gases (GHGs)**

521 Determination of the GHG time constants allows benchmarking of the chamber performance prior
522 to and after modifications. In both configurations the greenhouse gases CO_2 , CH_4 and N_2O were
523 anticipated to behave as non-reactive trace gases with little to no physical interactions on chamber
524 surfaces, nor to undergo chemical transformations.

525 The theoretical fill and empty rates for the chambers with a flow rate of $2\ L\ min^{-1}$ are 36 min. The
526 average measured time constants of filling wfor CH_4 , CO_2 , and N_2O in the unmodified chamber
527 were 37 ± 1 min, 37 ± 2 min, and 37 ± 1 min, respectively (Table 1). During emptying, they were
528 37 ± 1 min, 37 ± 1 min, and 38 ± 2 min, respectively. These measurements are not different from
529 theory within the limits of experimental accuracy (Figure 2). Since the GHGs are effectively
530 transferred through both the modified and unmodified configurations of the chamber, the baseline
531 performance of the chambers was not affected by the hardware modifications. Therefore,
532 comparison of these results with the time constants of N_r gases provides a description of their
533 interaction or transformation processes on the modified chamber surfaces.



534

535 **Figure 2.** Addition of reactive nitrogen gases and greenhouse gases to a modified dynamic
 536 chamber. For clarity, the coloured traces show the fitting curves corresponding to the response
 537 time in concentration normalized to the delivered value of each gas while filling and emptying the
 538 chamber. The black trace corresponds to a perfect non-reactive transfer of an ideal trace gas based
 539 on volume transfer in the chamber only. Note that the N₂O, CH₄, CO₂ and NO fill and empty traces
 540 all overlap with the theoretical fill and empty curves.

541

542 3.1.2 Time constants of reactive nitrogen gases

543 In the modified chamber, the time constant of filling or emptying with NO was 38 ± 1 min. The
 544 obtained NO time constants are similar to GHGs, as NO is not expected to have strong surface
 545 interactions. The slower time response of the NO₂, HONO, and NH₃ measurements is determined
 546 by two processes: (1) the exchange of the sample air volume in the gas transfer lines and the
 547 chamber, and (2) the adsorption and desorption of the gas onto and from their surfaces (Whitehead
 548 et al., 2008). Increases in the extent of surface interactions followed the increasing polarity,
 549 reactivity, and/or ionizability of gases in the order of NO₂, then HONO, and most for NH₃ (Figure
 550 2).

551 For example, NO₂ is lost more readily than NO, possibly through its known reaction on surfaces
552 to make HONO and HNO₃, being lost itself in the process (Finlayson-Pitts et al., 2003). It also has
553 higher water solubility than NO, but lower than for HONO or NH₃. Similarly, a decrease in
554 transmission efficiency for HONO could be explained by its weakly acidic nature (pK_a = 3.16)
555 (Silva et al., 2006) and solubility in water (Henry's law constant = 0.48 mol/m³ Pa; (Schwartz &
556 White, 1981) that facilitate partitioning and dissociation in surface water films, which could
557 generate non-volatile nitrite (NO₂⁻) on chamber surfaces. This chemistry will slow the transfer of
558 gas-phase HONO through the chambers, as the NO₂⁻ would need to protonate before being lost as
559 neutral HONO when repartitioning to the gas phase (R4, R5). Finally, the most delayed
560 transmission rate is for NH₃, likely because it undergoes strong inter-molecule interactions and
561 ionization on the chamber surfaces and/or any interfacial water (Henry's law constant = 5.9x10⁻¹
562 mol/m³ Pa (Orkin et al., 2011); pK_a = 9.25 (Lide, 2009), as well as on tubing surfaces and
563 potentially partitioning into the tubing before reaching the analyzer (Pagonis et al., 2017). The best
564 improvement in the time constants between the modified and unmodified configurations was 2.6
565 ± 2.5 min for HONO, with smaller improvements observed for NO₂ and NH₃ during the filling
566 process. Improved time constants when emptying reactive nitrogen from the chambers had similar
567 trends (Table 1). As a result, increasing delays from NO through NH₃ exist in our N_r gas suite due
568 to increasingly stronger interactions with chamber surfaces and gas handling lines.

569 The determined surface interaction values (D; Table 1; ES-2, Section S3) demonstrate an expected
570 greater impact of surfaces when no reactive gas is present in the headspace prior to filling, and a
571 lesser effect during emptying as the exposed surface has equilibrated with the analyte, which is
572 commonly referred to as passivation. For NH₃ specifically, the fill has a D value of 89%, while
573 during emptying it is only 23%, similar to our findings with NH₃ transfer for other N_r instruments
574 (Crilley et al., 2023). The surface interactions for these gases are minimized in the modified
575 chambers to facilitate more time-efficient measurements of surface exchange. However, they
576 necessitate the use of the λ term when deployed in the measurement-reference configuration for
577 those N_r species which experience partial transmission, such as NH₃. The λ term is required to
578 obtain accurate values, as the enclosed flux measurement surface should be perturbed for the least
579 amount of time possible when making field measurements, and the chambers cannot be closed for
580 several hours to allow surface-active gases to passivate the lines. One potential option to improve
581 the system performance further for NH₃ could be to heat the gas transfer lines between the

582 chambers and gas analyzers. In addition, minimizing the potential for transformations reduces the
 583 frequency required for in-field characterization of these processes through positive and negative
 584 gas delivery controls. For NO₂, specifically, we sought to quantify this as a function of modifying
 585 components of our chambers, as NO₂ is the most reactive gas in our suite (Section S5).

586 **Table 1.** Summary of time responses of addition and removal of GHGs and N_r gases to and from
 587 a chamber at 2 L min⁻¹ in unmodified and modified configurations. Time responses here
 588 correspond to a theoretical fill or empty e-folding time response of 36 minutes. Where analytes
 589 were observed to undergo surface interactions, a double exponential fit was used to characterize
 590 them, with the first time constant representing the known gas exchange rate being fixed at 36
 591 minutes, as this was observed for the non-reactive gases, and the second time constant is reported
 592 (*) alongside an assessment of the relative magnitude of surface interactions, through the D-value
 593 (%) (Crilley et al., 2023; Ellis et al., 2010; Moravek et al., 2019). Variability shown is one standard
 594 deviation of the mean from replicate experiments (n=3).

Gas species	Direction	Unmodified (min)	Modified (min)	Improvement (min)	D (%)
NO	Fill	38.8 ± 0.7	37.8 ± 0.6	1.0 ± 0.7	-
	Empty	37.9 ± 1.5	36.0 ± 0.6	1.9 ± 2.1	-
NO ₂	Fill*	18.9 ± 0.6	18.0 ± 3.1	0.9 ± 3.2	94 ± 18
	Empty*	21.2 ± 1.2	20.4 ± 1.4	0.8 ± 1.9	78 ± 21
HONO	Fill*	21.9 ± 1.1	19.3 ± 1.2	2.6 ± 1.6	74 ± 10
	Empty*	23.2 ± 1.4	21.2 ± 0.9	2.0 ± 1.7	71 ± 9
NH ₃	Fill*	69.6 ± 0.4	68.2 ± 0.5	1.4 ± 0.6	89 ± 3
	Empty*	76.9 ± 0.8	75.0 ± 4.6	1.9 ± 4.7	23 ± 4
CO ₂	Fill	37.9 ± 1.5	37.0 ± 1.8	0.9 ± 2.3	-
	Empty	38.0 ± 1.8	37.0 ± 1.2	1.0 ± 2.2	-
CH ₄	Fill	37.9 ± 1.1	36.8 ± 1.2	1.1 ± 1.6	-
	Empty	39.1 ± 1.7	37.2 ± 1.2	1.9 ± 2.1	-
N ₂ O	Fill	38.6 ± 2.1	36.7 ± 1.2	1.9 ± 2.4	-
	Empty	39.7 ± 1.3	37.7 ± 1.6	2.0 ± 2.1	-

595

596

597 **3.2 Multiplexer modification impacts on gas transfer**

598 The multiplexer (eosMX; Eosense Inc.) allows operation of up to twelve dynamic chambers
599 simultaneously with a suite of gas analyzers. However, it is constructed with stainless steel (SS)
600 valves and fittings that would be expected to facilitate strong interactions and/or losses of target
601 gases in the N_r analyte suite. Valves and fittings made of SS have a higher tendency to chemically
602 interact and/or adsorb reactive gases compared to fluoropolymer replacements. To address this
603 uncertainty, the gas transfer efficiency as a percentage loss in the multiplexer versus a bypass line
604 was evaluated specifically for NH_3 and NO_2 , alongside standard GHGs as they passed through
605 fittings and gas handling solenoid valves made of SS or PFA and PTFE replacement parts.

606 The loss fractions were modest and measurable when using minimal lengths of PFA tubing (~50
607 cm) instead of the standard 15 m gas transfer lines. The most substantial loss was observed on SS,
608 as expected due to its known tendencies (Vaaitinen et al., 2014). When the GHGs were delivered
609 for 30 minutes, typical of a chamber closure period in the field, their losses ranged from 10% for
610 N_2O to 19% for H_2O . Meanwhile, NO_2 exhibited 17% loss on the SS surfaces, and the greatest
611 effect was seen for NH_3 with a loss of 38% (Figure S6). In contrast, losses on the chemically inert
612 and hydrophobic surface of the PFA fittings and PTFE valve were negligible (<1%) for most gases,
613 except for NH_3 , which still exhibited a measurable loss of 11%. Other reports have also shown up
614 to 15% loss of NH_3 at atmospheric pressure on PTFE and PFA surfaces (Ellis et al., 2010; Shah et
615 al., 2006; Vaaitinen et al., 2014). While it is expected that the SS would eventually passivate and
616 improve the transmission of the GHGs in a standard recirculation approach, this is not likely to be
617 the case for destructively analyzed N_r and even more so if it facilitates a chemical transformation.
618 Overall, we found that replacing the multiplexer SS valves and fittings with PFA fittings and PTFE
619 valves provided a 9–27% reduction in surface losses of N_r compounds and GHGs. We strongly
620 recommend the use of PTFE and/or PFA materials over SS for more accurate measurement of N_r
621 species when interfacing the dual chamber setup with the destructive N_r analyzers needed for field
622 flux measurements, whether using a custom setup or the commercially available multiplexer.

623 **3.3 Minimizing NO_2 losses and determining controlling variables**

624 In addition to the rate of transfer of N_r gases, chamber modifications are necessary to prevent
625 reactive losses. These experiments enabled us to determine the magnitude of NO_2 lost to the
626 chamber and gas transfer tubing surfaces due to chemical and/or physical transformations, as well

627 as demonstrate the effectiveness of the different chamber modifications in minimizing these losses.
628 For NO₂, a probable chemical transformation pathway is its heterogeneous conversion to HONO
629 (R3), which is favourable under atmospherically relevant humidities, and the resulting water-
630 adsorbed surfaces expected to exist throughout the chamber and sampling lines.

631 **3.3.1. Chamber modification impacts on NO₂ losses**

632 . Substantial reduction in NO₂ loss fraction (f_{NO_2}) and transformation was observed from the
633 implemented PFA and PTFE modifications under conditions of 83% RH and 5 ppb of NO₂. In the
634 original unmodified configuration of the chamber, f_{NO_2} was 0.36 ± 0.02 (Figure S7) which was
635 reduced to 0.22 ± 0.03 with the PFA film, a relative decrease of 18%. This is consistent with the
636 acrylic chamber surfaces and fasteners to the chamber frame, facilitating physical and/or chemical
637 loss of NO₂.

638 The film of PFA, along with other fluoropolymers, is known to have excellent chemical resistance
639 and low reactivity towards a range of chemicals, including NO₂ (Ebnesajjad, 2005; Graham et al.,
640 1997). In addition, the superhydrophobic nature of these materials prevents the accumulation of
641 water on the surfaces, which is known to facilitate atmospheric surface reactions of NO₂
642 (Finlayson-Pitts et al., 2002; Jenkin et al., 1988; Stutz et al., 2002) and create analytical bias in the
643 measurement of trace gases like HONO, especially when instrument gas sampling inlets do not
644 take this into account (Crilley et al., 2019; Von Der Heyden et al., 2022).

645 The replacement of the brass-lined push-to-connect bulkhead fittings with PTFE led to a similar
646 decrease in f_{NO_2} , which was reduced by 17% to a final value of less than 0.05 ± 0.02 (Figure S7).
647 These fitting surfaces act as the largest surface-driven NO₂ loss despite their surface area being
648 very small compared to that of the entire chamber configuration and with a very small contact time
649 against the gas sample (0.012 s per fitting at a flow rate of 2 L min^{-1}).

650 The loss of NO₂ in the commercially available system is challenging to attribute solely to the
651 heterogeneous hydrolysis reaction. During the characterization experiments, the conditions inside
652 the chamber were matched to those reported by previous lab studies, which have shown that high
653 RH, presence of NO₂, and surface adsorbed water on surfaces favour this loss mechanism (Jenkin
654 et al., 1988; Stutz et al., 2004). The reaction is known to occur on surfaces such as Pyrex (Jenkin

655 et al., 1988) and borosilicate glass (Finlayson-Pitts et al., 2002), but no prior studies to date, nor
656 this study, have demonstrated metallic surfaces as facilitating this mechanism.

657 The inert PTFE fittings dramatically minimized transformations, while PFA film lining the inner
658 chamber surfaces was also effective, but less so. Our results indicate that water-adsorbed and
659 metallic surfaces, such as brass, facilitate substantial loss and/or transformations of NO₂. Further
660 investigation is required to confirm the mechanism(s) at play and is beyond the scope of this work.

661

662 **3.3.2. RH-facilitated NO₂ loss as a function of concentration**

663 A complete characterization of f_{NO_2} and the amount of HONO in the fully modified chamber was
664 determined under a range of environmentally relevant RHs and NO₂ concentrations. We found that
665 the absolute and fractional NO₂ losses were highest under the highest RH conditions (85%; Table
666 2). However, the f_{NO_2} does not appear to follow a concentration-dependent trend across the
667 additions made at lower RHs, with at most 0.4 ppbv NO₂ lost across the remainder of the tests, a
668 value which is equivalent to the LOD of the NO_x analyzer used. This would generate 0.2 ppbv of
669 HONO according to the disproportionation of the hydrolysis mechanism, which is well below the
670 analyzer detection limits. The modifications successfully reduced NO₂ losses below 10% across
671 all environmentally relevant conditions the chambers are expected to encounter, with our findings
672 here suggesting that the mass lost is nearly constant and independent of NO₂ mixing ratio at RHs
673 below 85%, while being marginally higher at and above this value.

674 Quantifying f_{NO_2} and the amount of HONO made in the chamber is required for the correction of
675 field datasets. The dual chamber system, via the RC, can also quantify any changes in these
676 processes over time if standard additions to the headspace are conducted. Consequently, important
677 parameters such as NO₂ deposition fluxes on surfaces can be better estimated (Pape et al., 2009).

678 Since the inferred HONO mixing ratios from the chamber surfaces across various environmental
679 RHs are nearly invariant at 0.2 ± 0.1 ppbv, it is simple to background correct any observational
680 datasets by subtracting this amount from the total HONO measured in the chamber. In addition, as
681 the NO₂ values expected in most atmospheric gas samples during field measurements are well into
682 the ppbv range (>3.3 ppbv per 30-minute flux measurement for a $0.08 \mu\text{g N m}^{-2} \text{hr}^{-1}$ emission), the

683 corrections would be easy to implement in post-processing of datasets and have minimal impact
 684 on the technical aspects of the analytical determinations.

685 **Table 2.** Characterization of NO₂ lost in the modified chamber under environmentally relevant
 686 ranges of NO₂ and RH. The loss fraction (f_{NO_2}) and HONO produced in the chamber were
 687 quantified. Variability (\pm) provided is one standard deviation of the mean from replicate
 688 experiments (n=3).

	RH (%)	NO ₂ added (ppbv)	NO ₂ lost (ppbv)	f_{NO_2}	HONO produced (ppbv)
689					
690					
691					
692	85	5	0.50 ± 0.01	0.1 ± 0.02	
693	85	7	0.70 ± 0.04	0.1 ± 0.02	
694					
695	85	10	0.50 ± 0.07	0.05 ± 0.01	
696					
697	65	5	0.30 ± 0.10	0.06 ± 0.02	
698					
699	65	7	0.40 ± 0.09	0.06 ± 0.02	<1.1 ^a
700					
701	65	10	0.30 ± 0.08	0.03 ± 0.01	
702					
703	45	5	0.30 ± 0.05	0.05 ± 0.01	
704					
705	45	7	0.40 ± 0.04	0.06 ± 0.00	
706					
706	45	10	0.30 ± 0.08	0.03 ± 0.01	

707 ^a – below instrument detection limit of 1.1 ppbv determined as S/N=3 while sampling zero air

708 It should be noted that the amount of HONO in the chamber was below the LOD of the NO_x
 709 analyzer for HONO (1.1 ppbv), meaning that the upper limit of HONO inferred may perhaps, in
 710 fact, be negligible. Therefore, future experiments that wish to detect small N_r fluxes accurately
 711 will need to focus on reproducing these experiments with a higher performance instrument, such
 712 as a time-of-flight chemical ionization mass spectrometer (ToF-MS) or long-path absorption
 713 photometer (LOPAP), which have lower detection limits (Crilley et al., 2019; Lee et al., 2014;
 714 Neuman et al., 2016; Reed et al., 2016).

715 3.3.3 Loss of O₃ with and without fluoropolymer modifications

716 Ozone loss was observed in both modified and unmodified chamber configurations, with 18% lost
 717 to clean 15 m PFA lines alone when transferring 30 ppbv. The unmodified chambers lost 45%
 718 across delivered mixing ratios spanning 150-250 ppbv.. This was reduced to 35% when the
 719 fluoropolymer modifications were implemented. When the PFA film was aged by 15 days of

720 ambient sampling and 2 years of exposure to lab air, the losses were substantially exacerbated,
721 reaching 80%. Such outcomes are expected and can be attributed to several factors discussed in
722 detail in Section S5, primarily involving surface reactions with built-up films of deposited
723 organics, adsorption, and material interactions (Burkholder et al., 2015, Ebnesajjad, 2017, George
724 et al., 2015, Plake et al., 2015). We recommend regular replacement of the PFA film as part of the
725 N_r system maintenance, coupled with quality control procedures to characterize material
726 performance for target gases.

727

728 **3.3 Proof-of-concept reactive nitrogen fluxes using soil samples in the lab**

729 Proof-of-concept flux measurements were performed using the modified dynamic chamber system
730 to demonstrate that emissions of N_r gases from agricultural soil samples can be measured under
731 controlled conditions, similar to many prior reports using custom-built soil chambers (Almand-
732 Hunter et al., 2015; Pape et al., 2009; Tang et al., 2019, 2020).

733 **3.3.1. Fluxes of NO, NO₂, and HONO from agricultural soil samples**

734 Emission fluxes were measured from two pooled and two individual soil samples collected from
735 a single agricultural field (Table 3; Section S6). The average and integrated fluxes of N₂O, NH₃,
736 NO, NO₂, and HONO were assessed under controlled, environmentally realistic (65 % RH), drying
737 conditions (Table 3).

738 As the soils dried, NO and NO₂ emissions increased, with NO fluxes highest across all replicates
739 and reaching up to 2.50 μg N m⁻² hr⁻¹. This trend is consistent with the prior work of other
740 researchers, showing peak NO emission potentials when VWC drops below 25% during soil
741 drying, which is when microbial nitrification and denitrification processes are suggested to become
742 more active (Bao et al., 2022; Oswald et al., 2013). The soil VWC at which these maxima occur
743 can vary depending on soil type, texture, and microbial diversity therein (Ludwig et al., 2001;
744 Schindlbacher et al., 2009). Plot-level replicates from our field had a higher integrated NO flux
745 (i.e., > 2600 μg N m⁻²), compared to the pooled replicates (<1000 μg N m⁻²), likely indicating real
746 differences in preserved microbial hotspots, intact plot-level soil aggregates, true spatial
747 variability, and plot-specific N availability (Table 3). Soil texture and aggregate size, for example,
748 play an important role in building the porous structure of soil, which has implications for the

749 release of gases (Mangalassery et al., 2013). Soil aggregates, therefore, govern the release of
750 gaseous N_r analytes like NO based on the aerobic or anaerobic state of the soil. Here, our low level
751 of soil manipulation (i.e. not ground, no sieving) will drive some of the variability by preserving
752 these features, which exist across and within real soil systems (Lipiec et al., 2007). Individual plot
753 samples also retain plot-specific microbial communities when working with intact soil, whereas
754 soil grinding can temporarily inhibit microbial activity. While we tried to minimize soil handling
755 and processing extremes in these experiments, a measure of homogeneity was also pursued, and
756 fully intact soil cores were not assessed.

757 Integrated NO₂ fluxes showed the same trend, with more sample-to-sample variability as one
758 pooled replicate (R2) produced over three times the emissions of R1, despite both experiments
759 being conducted across identical moisture content ranges (Table 3). Given the limited studies
760 directly measuring NO₂, such as Purchase et al. (2023), this variability is difficult to interpret and
761 highlights the need for more assessments of its production pathways and controls, which our
762 developed chambers show promise for.

763 The observed average HONO fluxes remained low across all of the samples, ranging from 0.05 to
764 0.25 μg N m⁻² hr⁻¹ (Table 3). These values are lower by more than an order of magnitude compared
765 to those reported in other controlled laboratory studies, where HONO fluxes exceed 900 μg N m⁻²
766 hr⁻¹ (Oswald et al., 2013; Su et al., 2011; Wang et al., 2021). These discrepancies are concerning,
767 given recent emphasis from the scientific community on the atmospheric impacts of soil-derived
768 HONO on air quality. Here, the results from our agricultural soil samples may reflect the
769 differences in our methodology, such as the soil handling and preparation steps prior to and during
770 experiments. Many prior reports prepare their samples in ways that strongly deviate from real-
771 world conditions (e.g. initial soil drying temperatures above those occurring under ambient
772 conditions, extreme storage conditions, grinding, sieving, use of dry zero air to flush chambers,
773 etc.). Further drivers of variability within the category of heavily altered soil samples from the
774 literature include pH, NO₂⁻ availability, and NH₄⁺ or NO₃⁻ content, all of which are known to
775 influence biotic and abiotic HONO formation pathways (Wu et al., 2019).

776 Our HONO fluxes from the agricultural soil samples studied here are consistent with field
777 observations under ambient conditions, where average emissions have been reported to largely
778 remain below 7.2 μg N m⁻² hr⁻¹ (Tang et al., 2019; Xue et al., 2024). This does suggest that greater

779 care in sample preparation, and likely also a widely agreed-upon standard procedure, is needed to
780 study soil HONO emissions relevant to atmospheric models.

781 The integrated HONO fluxes for the pooled replicates yielded $185 \mu\text{g N m}^{-2}$ and $146 \mu\text{g N m}^{-2}$,
782 respectively. From the individual sample replicates, which were slightly wetter than the pooled,
783 the integrated HONO fluxes were 690 and $739 \mu\text{g N m}^{-2}$, which was unexpected because the
784 overall moisture regime accessed by the pooled soil experiments was not lower than those from
785 the plot samples. The drier soils would have been expected to yield greater integrated HONO
786 emissions (Oswald et al., 2013), yet this was not the case. Additional replicates and experimental
787 controls, while beyond the scope of this study, would allow further attribution of the controls over
788 the observed HONO variability.

789 **Table 3.** Average and integrated fluxes of NO, NO₂, and HONO (in $\mu\text{g N m}^{-2} \text{hr}^{-1}$ and $\mu\text{g N m}^{-2}$, respectively) from agricultural soil
 790 samples across two soil VWC ranges. Both the average and integrated fluxes were calculated over a constant period within the noted
 791 range of soil VWC. Values are reported as mean \pm standard error.

Soil sample	Soil VWC Range (%)	Duration (hr)	Avg Flux ($\mu\text{g N m}^{-2} \text{hr}^{-1}$)			Integrated flux ($\mu\text{g N m}^{-2}$)		
			NO	NO ₂	HONO	NO	NO ₂	HONO
Pooled R1	16-22	125	1.0 \pm 0.04	0.05 \pm 0.02	0.06 \pm 0.02	2400 \pm 120	160 \pm 50	190 \pm 50
Pooled R2	16-22	125	1.0 \pm 0.04	0.20 \pm 0.02	0.05 \pm 0.01	2500 \pm 130	500 \pm 60	150 \pm 40
Plot R1	22-27	65	1.2 \pm 0.05	0.40 \pm 0.03	0.20 \pm 0.02	3400 \pm 150	1300 \pm 90	690 \pm 70
Plot R2	22-27	65	1.0 \pm 0.03	0.50 \pm 0.04	0.30 \pm 0.02	2600 \pm 100	1600 \pm 100	740 \pm 50

792

793 These findings demonstrate the utility of the modified custom-built dynamic chambers for
794 accurately capturing N_r fluxes under controlled laboratory settings, but they also highlight the need
795 for more such systems to be implemented across the scientific community to better consider both
796 biogeochemical soil properties and environmental context when interpreting the impacts of N_r
797 fluxes obtained in the lab and scaling them to real soils. There seems to be potential for skewing
798 the atmospheric impacts as a result, in particular for HONO, as the standard approaches have been
799 designed to replicate NO fluxes (Behrendt et al., 2014). Most global models do not consider the
800 effect of soil HONO on air quality through O_3 production and oxidation chemistry [Click or tap here](#)
801 [to enter text.](#) Several modelling studies like Ha et al. (2023) and Tian et al. (2024) have
802 incorporated the order of magnitude or higher HONO fluxes reported from lab studies, like those
803 by Su et al. (2011), Wang et al. (2021), Oswald et al. (2013), and Meusel et al. (2018). They
804 estimated significant HONO production with maximum flux potentials of $830 \mu\text{g N m}^{-2} \text{hr}^{-1}$, $95 \mu\text{g}$
805 $\text{N m}^{-2} \text{hr}^{-1}$, $70 \mu\text{g N m}^{-2} \text{hr}^{-1}$, $55 \mu\text{g N m}^{-2} \text{hr}^{-1}$, respectively. In contrast, the field observations that
806 do exist suggest that real HONO fluxes are much smaller at $2\text{-}17.5 \mu\text{g N m}^{-2} \text{hr}^{-1}$ (Song et al., 2023;
807 Tang et al., 2019). Similarly, Wu et al. (2022) has used the regional WRF-Chem model to explore
808 the impact of soil HONO emissions on the concentrations of atmospheric HONO, OH, and O_3 .

809 Agricultural soil HONO emissions have been suggested to significantly contribute to OH radical
810 production, accounting for approximately 10% to 60% of total OH formation in rural areas before
811 noon (Oswald et al., 2013; Su et al., 2011), which often exceed the contributions from ozone
812 photolysis. Additionally, high HONO emissions from agricultural soils have been reported to
813 increase local O_3 concentrations by $\sim 0.5 - 1.0$ ppb in low- NO_x rural environments where VOCs
814 are not limiting (Zhang et al., 2021), with even greater impacts observed during fertilization
815 periods (Wu et al., 2022). Modelling studies, using GEOS-Chem and CMAQ, for example, claim
816 that incorporating soil HONO emissions improves the agreement between observed and simulated
817 O_3 levels, particularly during the morning (Zhang et al., 2021).

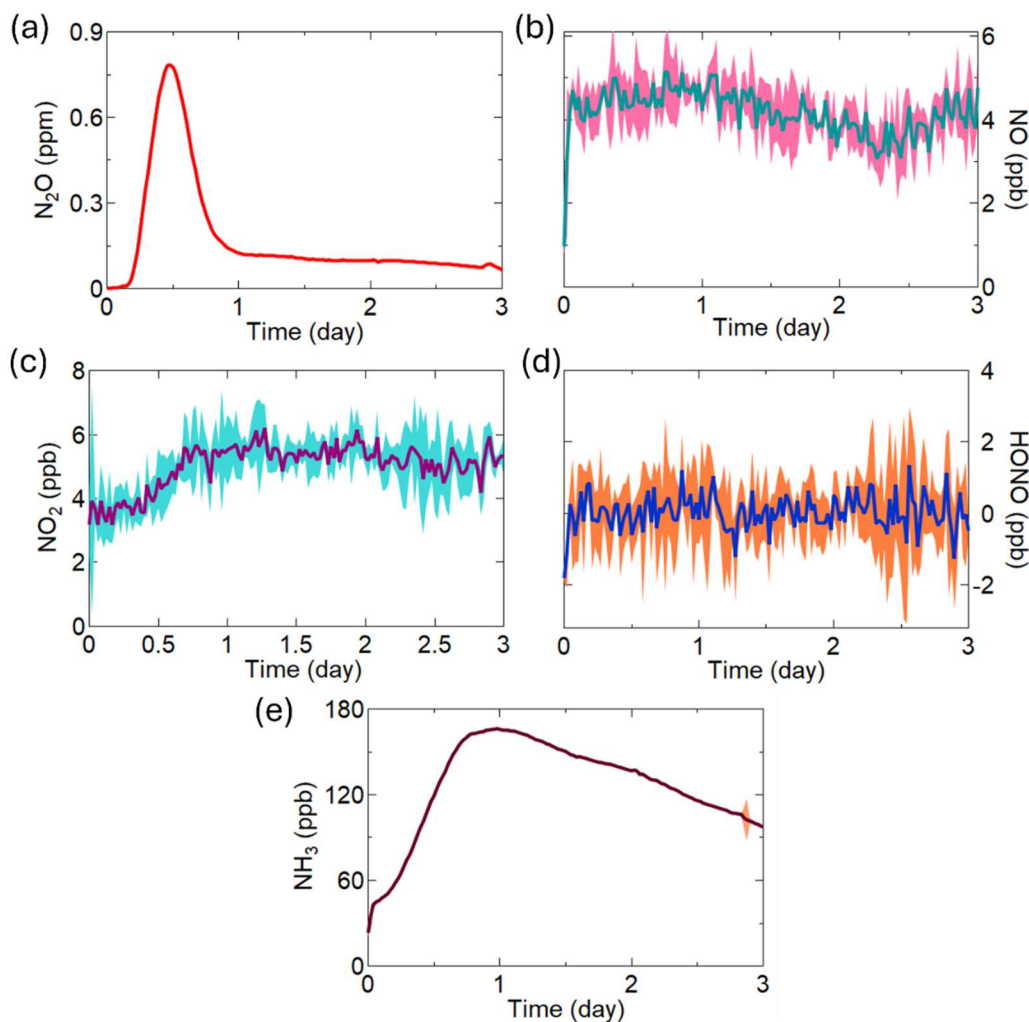
818 Only a few studies have conducted estimates of soil NO_x emissions under reasonable conditions,
819 like Bao et al. (2022) and Wu et al. (2022), where the researchers tried to mimic field conditions.
820 Even in such an area that has been long studied, large uncertainty still exists around soil sources
821 of NO_x , particularly for agricultural activities where uncertainty is still at least $\pm 30\%$ due to
822 limitations in lab characterizations and field experiments (Gong et al., 2025). It is not surprising,

823 then, that a similar issue exists for the very recent work on HONO soil emissions. The NO_x
824 uncertainty range results from intricate soil biogeochemical processes and varies with crop types,
825 soil texture, fertilizer types and application rate (Gong et al., 2025). This longstanding and
826 established difficulty in predicting soil NO_x for use in global chemical models means that doing
827 so for HONO without careful ground truthing of real-world emissions could lead to substantial
828 inflation of the impacts on atmospheric chemistry and air quality. Care should be taken in using
829 HONO emissions from lab studies in global models, as it seems they pose a risk of overestimating
830 their atmospheric impacts until a more representative experimental design can be obtained with
831 chamber systems like the one used here.

832 **3.3.2 Fluxes of N_r from fertilized agricultural soil samples**

833 Agricultural soils amended with chemical fertilizers are expected to be hotspots for NH₃, N₂O,
834 HONO, and NO_x emissions. Here, we demonstrate the use of our developed chambers to measure
835 these analytes under controlled lab conditions using our lightly processed pooled soil samples and
836 four fertilizers: urea, ammonium nitrate (AN), ammonium bicarbonate (ABC), and ammonium
837 carbonate (AC) with the temperature maintained at 23 °C, VWC between 25–29%, and headspace
838 RH held at 65% for three days, simulating realistic atmospheric and environmental N_r flux
839 exchange conditions following farm field fertilization (Figure 3). In all experiments conducted
840 with the Picarro G2509, the mixing ratio of N₂O began to rise approximately four hours after the
841 experiment started. In the example shown for urea, it peaked at 0.79 ppm after 12 hours, which
842 was followed by a gradual decline (Figure 3a). This pattern likely reflects the incubation period of
843 nitrifying and denitrifying bacteria that leads to the subsequent release of gases like HONO, as
844 depicted in Wang et al. (2021), and N₂O in Liu et al. (2022). In contrast, the mixing ratio of NO
845 remained relatively constant throughout the three days (Figure 3b), with NO₂ increasing as the
846 N₂O emissions decreased, while NO was emitted constantly throughout (Figure 3c). In this
847 example experiment, no measurable emissions of HONO were detected despite the substantial
848 presence of urea and evidence of active microbial nitrification and denitrification from the other
849 emitted gases (Figure 3d). Lastly, the urea application example in Figure 3e shows the expected
850 significant NH₃ emissions, with the integrated amount reaching 22% of the applied N over the
851 three-day incubation period. These findings are consistent with our existing knowledge that NH₃
852 volatilization as an N loss mechanism dominates early N_r losses from fertilizers.

853 Volatilization of NH_3 is well-characterized as a major pathway for N loss from fertilizers (Behera
 854 et al., 2013; Govoni Brondi et al., 2024; Liu et al., 2020; Moravek et al., 2019; Pan et al., 2016,
 855 2022; Paulot et al., 2014). Besides agronomic concerns due to N loss and reduced fertilizer
 856 efficiency related to NH_3 emissions from fertilized soil (Anas et al., 2020), it is a key precursor to
 857 secondary inorganic aerosols in the atmosphere with impacts on respiratory and ecosystem health,
 858 visibility, and climate (Dennis et al., 2010; Edwards et al., 2024; Fowler et al., 2013; González
 859 Ortiz et al., 2020; Jang et al., 2025; Seinfeld and Pandis, 2006).



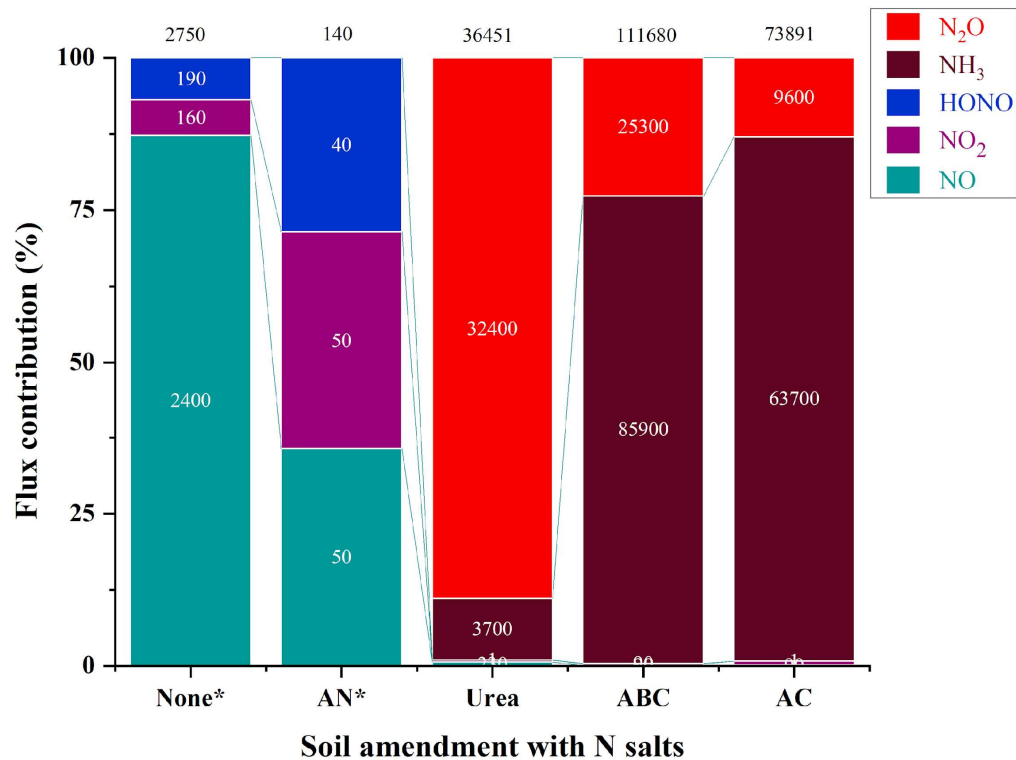
860
 861 **Figure 3.** Soil emissions of the comprehensive suite gases from soil treated with urea, including
 862 (a) N_2O ; (b) NO ; (c) NO_2 ; (d) HONO ; and (e) NH_3 . The NO , NO_2 and HONO emissions were
 863 measured at 1-minute resolution and averaged to 30 min. The standard deviation ($\pm 2\sigma$) around
 864 these averages is shaded with a lighter version of the main trace colour. Similarly, the 2-second
 865 resolution of N_2O and NH_3 measurements were also averaged to 30-minute intervals with $\pm 1\sigma$
 866 provided in shading.
 867

868 Emissions of NH_3 and N_2O were observed to be far greater in terms of integrated amounts from
869 the fertilized samples (Figure 4). Integrated flux for NH_3 produced by soil treated with ABC
870 accounted for 77% of total N_r flux (i.e., $85\,900\ \mu\text{g N m}^{-2}$), followed by AC, which was $63\,700\ \mu\text{g}$
871 N m^{-2} . This is not surprising, since the use of chemical fertilizers increases the concentration of
872 NH_4^+ in the soil that can deprotonate to emit neutral NH_3 and, in the presence of ammonia-
873 oxidizing microorganisms, increases the production of N_2O (Luo et al., 2025). Nitrous oxide
874 released from the addition of urea accounted for the highest integrated flux of $32\,400\ \mu\text{g N m}^{-2}$
875 observed, representing 89% of total N_r released, followed by $25\,300\ \mu\text{g N m}^{-2}$ and $9\,600\ \mu\text{g N m}^{-2}$
876 for ABC and AC, respectively. One way that has been proposed to reduce these large N_2O
877 emissions from inorganic fertilizers is to change the application form to organic fertilizer, as the
878 NH_4^+ in soil is produced more slowly (Luo et al., 2025). Due to a limited duration of access to the
879 G2509 to conduct this work, we were unable to measure the N_2O and NH_3 emitted from
880 unamended soils or those treated with AN. Regardless, based on the obtained data, the values
881 found here are similar to those observed under real environmental conditions (Figure 4). For our
882 sample without N amendment, the integrated flux of NO was the largest ($2\,400\ \mu\text{g N m}^{-2}$; 87% of
883 total NO_y), followed by comparable levels of NO_2 ($160\ \mu\text{g N m}^{-2}$) and HONO ($190\ \mu\text{g N m}^{-2}$). The
884 fluxes of NO_x and HONO were below $1\ \mu\text{g N m}^{-2}\ \text{hr}^{-1}$ for all the nutrient addition treatments,
885 suggesting a similar trend as those observed under field conditions and from our lab results with
886 unamended soils (Figure 4, Table S1, Section S6). The exact mechanism behind the HONO
887 release, being due to nitrification and/or denitrification, cannot be definitively assigned based on
888 flux data alone, and many factors drive these emissions. There are discrepancies still observed
889 between HONO flux measured from the treated soil samples in the laboratory and similar
890 measurements in literature (Oswald et al., 2013; Su et al., 2011), some of which report fluxes of
891 up to $\sim 3\,600\ \mu\text{g N m}^{-2}\ \text{hr}^{-1}$ and are likely overestimating the soil N_r fluxes found in the real world.
892 In contrast, our results are in close agreement with the field-based measurements of Tang et al.
893 (2020), which also used a dynamic chamber flux method.

894

895 These in-lab experiments show that simultaneous speciated N_r emissions towards mass balance
896 analysis in a controlled environment can be conducted using a single chamber and potentially
897 applied to an array of chambers, as others have done for a subset of gaseous N_r (Scharko et al.,
898 2015; Tang et al., 2019). With the limited replicates we explored here, our results raise a question

899 for researchers who have been using lab studies as a standard to predict and incorporate HONO
 900 soil emission values in particular into regional and global models.

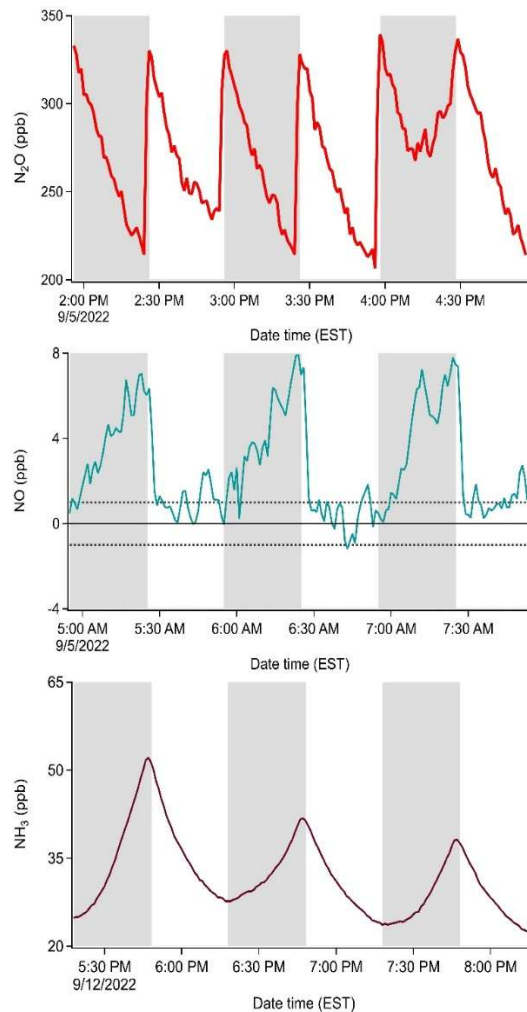


901
 902 **Figure 4.** Relative flux contribution of soil treated with four different nitrogen-containing fertilizer
 903 salts. Each segment shows the proportion of integrated flux of NO (cyan), NO₂ (purple), HONO
 904 (blue), NH₃ (brown) and N₂O (red), with discrete flux values presented in white text, and the total
 905 flux provided in black text above the column ($\mu\text{g N m}^{-2}$). Some samples (denoted by *) were only
 906 characterized for fluxes of NO, NO₂ and HONO using the modified NO_x analyzer, as the duration
 907 of our access to the G2509 for NH₃ and N₂O measurements was limited.

908
 909 **3.3.3 Dual chamber field deployment for automated continuous dynamic fluxes**

910 A pilot scale field campaign was carried out to demonstrate the application of our dual soil flux
 911 chambers in capturing N_r gas exchange processes. A paired MC and RC setup was deployed in the
 912 same field a year after the soil samples were collected for our lab experiments. During a period of
 913 stimulated N_r emission from an experimental application of urea in situ, the mixing ratios of NO,
 914 N₂O, and NH₃ were impacted compared to the unfertilized state. The changes within both the MC
 915 and RC were measured and used to calculate fluxes (Figure 5). The purpose of Figure 5 is
 916 methodological to demonstrate how rate, dilution, and reaction terms combine in the observed
 917 rates of concentration change during chamber cycles. The selected data for NH₃ correspond to

918 measurements taken after the fertilization event, while the selected NO and N₂O data segments are
919 examples for separate observations times which best demonstrated the contributions of all terms
920 prior to the fertilization event. Taken together, these three separate examples for the mathematical
921 terms in E6 and E7 contributing to the net flux can be considered more easily – they are entirely
922 ascribed to the rate term otherwise. Each set of observations span three consecutive hours of
923 dynamic changes in gas concentrations within the chambers which allow fluxes to be calculated.
924 For the 0.5 Hz measurement rate of the Picarro, it is clear from the accumulation and depletion of
925 target gases in Figure 5, that a shorter observation period than 30 minutes could be used when high
926 time resolution instrumentation across all target species is available. The benefit of this would be
927 to reduce both the alteration of the composition of the chamber headspace and diverging physical
928 conditions between the chamber and ambient environment; ultimately obtaining better flux
929 estimates. However, for this pilot study, the 1-minute time resolution of the NO_x analyzer and the
930 method for determining HONO by difference with an annular denuder every 5 minutes required
931 the 30-minute interval. A shorter closure period could also have the drawback of worse flux
932 detection limits when fluxes are small, and more variability due to a less robust regression of the
933 accumulation or depletion rate. For example, this would increase the value of λ for NH₃ (Figure
934 S11; Section S7) and its relative error (4% for a clean system, Section S7.3) as well as other
935 surface-interacting gases.

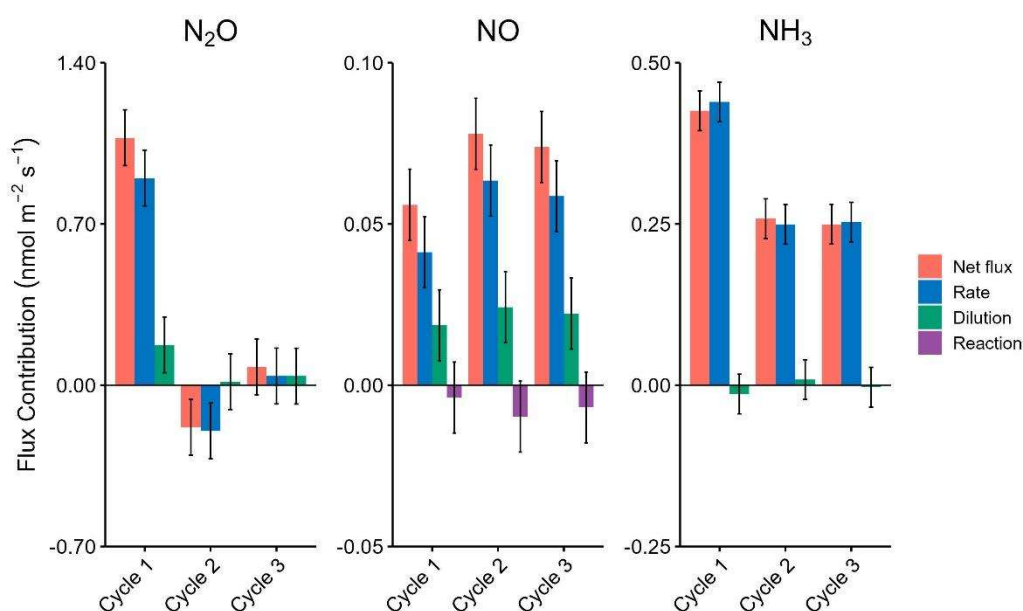


936

937 **Figure 5.** Mixing ratios of N_2O (ppb), NO (ppb), and NH_3 (ppb) in the measurement (grey shading)
 938 and reference (unshaded) chambers from three consecutive cycles during the pilot field study.
 939 Cycles are shown for representative, non-simultaneous periods to illustrate term contributions. The
 940 NH_3 cycles correspond to measurements taken after the fertilization perturbation, while the NO
 941 and N_2O cycles are from the same period before fertilization. The dashed lines for the NO
 942 measurements indicate ± 1 ppb (3σ noise), where the positive boundary represents the detection
 943 limit of the NO_x analyzer.

944 The breakdown of the flux components for NH_3 , N_2O , and NO can allow the contributions of the
 945 experimental setup (e.g. dilution) and environmental factors (e.g. reaction) to be considered
 946 independently (Figure 6). We consider these across a consecutive triplicate of flux determinations
 947 from the pilot field deployment, to provide meaningful examples. The uncertainty in each term is
 948 estimated from the variance between the triplicate of consecutive MC and RC observations,
 949 through the measured slopes (i.e. using E6 or E7) and assumes that ambient atmospheric
 950 composition did not change substantially during this error derivation period.

951 The rate term (dC/dt) is the dominant contributor to the determined flux for all three gases (Figure
 952 6), which are all positive and indicate emissions despite their clearly differing temporal trends.
 953 Each contribution term is defined and discussed in further detail in Section S7. Accurate
 954 quantification of trace gas fluxes using dynamic chamber systems requires correction for
 955 attenuation caused by surface interactions. These effects can significantly suppress the measured
 956 accumulation rate of reactive species within the closed MC (Figure 5). To account for the, the
 957 attenuation factor (λ) was introduced in this work (ES12), defined as the ratio of the theoretical
 958 concentration signal for an inert gas (e.g. as in our fill/empty experiments) to the measured signal
 959 over the chamber closure period. The value of λ is gas-specific and time-dependent, reflecting wall
 960 affinity and kinetics. This correction reduces flux bias, independent of chamber-specific losses.
 961 The highest attenuation was observed for NH_3 , for which a λ of 5.40 was determined empirically
 962 for the 30-minute closure period. Comparative values for NO_2 and HONO are also provided in
 963 Section S7.3.



964
 965 **Figure 6.** Contributions of different terms (rate, dilution, and reaction) to the net flux of NO , NH_3 ,
 966 and N_2O across three consecutive cycles ($\text{nmol m}^{-2} \text{s}^{-1}$). The rate represents the change in
 967 concentration measured over time, the dilution represents the integrated loss to dilution, and the
 968 reaction represents the contribution of known reactions happening inside the chamber. Error bars
 969 are calculated using the standard deviation about the mean of the corresponding terms from three
 970 consecutive chamber cycles. For visual clarity, the attenuation correction ($\lambda = 5.40$) for NH_3 is not
 971 applied in this figure, as it constitutes a linear scaling factor across all NH_3 bars (Section S7.3).

972 For N₂O, the first cycle exhibits the highest flux (1.07±0.12 nmol m⁻² s⁻¹), while the second cycle
973 showed uptake by the soil (-0.18±0.12 nmol m⁻² s⁻¹), and the final cycle showed no net flux within
974 error (0.08±0.12 nmol m⁻² s⁻¹). This occurs for a non-reactive greenhouse gas like N₂O despite the
975 concentration decreasing with time for both the measurement and reference periods, as the rate of
976 decrease during the measurement cycle is slower than that from dilution alone (Figure 6). Across
977 the three cycles, the rate of concentration change term contributed 84±15% to the measured flux
978 in the first cycle, 109±98% in the second cycle, and 50±171% in the third cycle. The negative rate
979 of concentration change in all of the observation periods arises due to the use of N₂O-free purge
980 gas delivered to the chamber headspace, which is required for the gas sample to be destructively
981 quantified, while not introducing ambient air into the chamber (Figure 5). This simultaneously
982 prevents sudden changes in local outdoor air composition from making small fluxes difficult to
983 detect, as well as reduces the uncertainty in the fluxes assigned. Here, the dilution terms range
984 from 8 to 50% of the net flux, as would be expected from the N₂O exchange switching from
985 emission to deposition during the three-cycle example (i.e. 3 hours). In the final measurement
986 cycle, the rate of concentration change transitions from a loss to steady state during the observation
987 period, suggesting that an instant of ‘hot spot, hot moment’ emission of N₂O was likely occurring.
988 As such, the transition leads to no net flux for the observation period, which is a limitation of our
989 dual-chamber approach compared to one with recirculating headspace, or that of an eddy
990 covariance approach that can capture higher temporal resolution changes in concentration. The
991 N₂O fluxes observed here are consistent with those reported for European arable soils using both
992 dynamic and static chambers, where event-driven N₂O peaks after fertilization commonly range
993 between 0.2 and 2.4 nmol m⁻² s⁻¹, and background periods can be as low as 0.08 nmol m⁻² s⁻¹
994 (Kong et al., 2025, Murphy et al., 2022, Maier et al., 2024, Manco et al., 2025). Field-scale eddy
995 covariance studies, such as Maier et al. (2022), have captured post-harvest pulses up to 1.6 nmol m⁻²
996 s⁻¹, highlighting the capacity of EC to resolve large, rapid emission events that single-point
997 chamber systems may miss. However, dynamic chamber systems provide high-precision,
998 temporally resolved flux data under controlled conditions, enabling direct attribution of emissions
999 to specific soil management or environmental factors (Butterbach-Bahl et al., 2013; Kong et al.,
1000 2025). This makes dynamic chambers, like those demonstrated here, especially valuable for
1001 mechanistic and process-level studies.

1002 For NO, the only gas we consider in the examples here with a reaction term, the reaction
1003 contribution is the smallest among the three flux components. Over all three cycles, the reaction
1004 term opposed the net flux by less than 13%. The magnitude of the reaction term is always
1005 negligible, remaining within the $\pm 0.01 \text{ nmol m}^{-2} \text{ s}^{-1}$ variability caused by background correction
1006 from the RC. Instead, the time rate of change in concentration term drove 74–81% of the total flux
1007 for all three cycles and dilution accounted for the remaining 30–33%. The reaction term falling
1008 within the uncertainty range of no contribution in all three cycles (e.g. $-0.01 \pm 0.01 \text{ nmol m}^{-2} \text{ s}^{-1}$ in
1009 the second cycle, where it had the greatest potential), indicates that its contribution is less certain
1010 than the other flux components as it is driven by the presence of O_3 , which is rapidly lost upon
1011 chamber closure. Overall, the low contribution of the reaction term suggests this process has a
1012 minor role in measured NO fluxes. In other, more polluted regions, such as the North China Plain
1013 (NCP) and the Pearl River Delta (PRD), where summertime ambient O_3 concentrations range from
1014 60 to 275 ppbv, the exceedances above 200 ppbv during pollution episodes (Wang et al., 2017)
1015 could make this term very important. As noted above, the PFA film on the chamber surface will
1016 change its properties with respect to O_3 transmission over time, highlighting the utility of the RC,
1017 which is designed to accumulate the same atmospheric compounds as the MC over time on all
1018 sampling surfaces.

1019 The resulting emission fluxes of NO observed in these three cycles were $0.056\text{-}0.078 \text{ nmol m}^{-2} \text{ s}^{-1}$
1020 ¹, which are well within the range reported for agricultural soils in North America and Europe,
1021 such as Taylor et al. (1999) who observed $-0.07\text{-}4.2 \text{ nmol m}^{-2} \text{ s}^{-1}$ in Canadian fertilized cropland,
1022 and Pape et al. (2009) and Almand-Hunter et al. (2014) who reported values of $0.05\text{-}4.0 \text{ nmol m}^{-2}$
1023 s^{-1} , using dynamic chambers in grass and cropland soils. Therefore, in the case of NO for this
1024 example, the variability in the fluxes is largely driven by real fluctuations in the rate term. This
1025 highlights the sensitivity of the total flux to changes in the rate of concentration change, and the
1026 precision of the method, as the uncertainty in the final fluxes here is on the order of 14%. Compared
1027 to the dynamic chambers reported by these prior studies, the RC in our dual-chamber system offers
1028 a clear advantage by directly correcting for baseline fluctuations and environmental drift that can
1029 confound single-chamber approaches. This is especially important for reactive gases such as NO,
1030 which are susceptible to rapid loss to O_3 and short-term background variability (Taylor et al.,
1031 1999). The dual-chamber system provides more robust, artifact-free quantification of soil–
1032 atmosphere exchange and is less susceptible to interference from transient local emissions (e.g.

1033 from nearby traffic or agricultural equipment) than single-chamber systems. In comparison to eddy
1034 covariance or flux-gradient techniques, which integrate over larger areas but may underestimate
1035 true NO fluxes due to post-emission chemistry (Taylor et al., 1999; Plake et al., 2015), our
1036 approach yields high-frequency, process-resolving data ideal for mechanistic and plot-scale
1037 studies.

1038 For NH₃, the rate of change term dominates the total flux, contributing $103 \pm 10\%$, $97 \pm 16\%$, and
1039 $101 \pm 17\%$ of the flux in cycles one, two, and three, respectively, while the dilution term
1040 contributes inconsequentially at $-3 \pm 7\%$, $3 \pm 12\%$, and $-1 \pm 12\%$ in the same three cycles,
1041 respectively. The resulting emission fluxes of NH₃ observed across these cycles ranged from
1042 $0.43 \pm 0.03 \text{ nmol m}^{-2} \text{ s}^{-1}$ in cycle one down to $0.25 \pm 0.03 \text{ nmol m}^{-2} \text{ s}^{-1}$ in cycle three. The relatively
1043 small contribution of the dilution term is consistent with the expectation that the RC and MC
1044 exhibit similar dilution effects. The relative uncertainty in the final NH₃ fluxes is 7% for cycle one,
1045 and 12% for cycles two and three. By comparison, relative uncertainties were 14% for NO and
1046 ranged from 15% to 171% for N₂O, reflecting the greater variability and lower precision associated
1047 with the smaller flux magnitudes for those gases.

1048 Our observed NH₃ fluxes ($0.25\text{--}0.43 \text{ nmol m}^{-2} \text{ s}^{-1}$) are consistent with literature values for managed
1049 grass and croplands. For instance, Milford et al. (2009) reported bi-directional background fluxes
1050 from -3.8 to $2.5 \text{ nmol m}^{-2} \text{ s}^{-1}$ prior to cutting intensively managed grassland, with larger diurnal
1051 emissions up to $42 \text{ nmol m}^{-2} \text{ s}^{-1}$ after cutting and maxima up to $224 \text{ nmol m}^{-2} \text{ s}^{-1}$ following fertilizer
1052 application. Abdulwahab et al. (2024) observed highly variable fluxes in intensively grazed French
1053 grassland, ranging from -6.6 to $188 \text{ nmol m}^{-2} \text{ s}^{-1}$, with short-lived maxima above $300 \text{ nmol m}^{-2} \text{ s}^{-1}$
1054 after slurry application, though most measurements were at much lower magnitudes. Notably,
1055 accurate quantification of NH₃ fluxes in this system critically depends on the application of the
1056 chamber-specific attenuation factor λ (Section S.7.3; Figure S11). Without this correction, true
1057 NH₃ fluxes would be underestimated by more than fivefold in our study. While the RC correction
1058 plays a role in the flux calculations, its impact on NH₃ is less pronounced than on N₂O, where the
1059 correction significantly alters the net flux direction (Figure 5; first cycle). Chamber-based
1060 approaches such as ours provide a key advantage for NH₃ over micrometeorological methods like
1061 eddy covariance, which are especially prone to high-frequency attenuation and chemical
1062 interferences for reactive gases. As shown in Moravek et al. (2019), even state-of-the-art closed-

1063 path EC systems may recover less than half (as little as 46%) of true NH₃ fluxes due to instrument
1064 limitations and turbulence losses. Challenges were also evident for relaxed eddy accumulation,
1065 where Xu et al. (2010) found that turbulence and surface effects complicated flux interpretation in
1066 cropland. Related methodological considerations have also been noted in other contexts.
1067 Schlossberg et al. (2017) highlighted how airflow and canopy structure can influence chamber
1068 NH₃ fluxes in turf systems, underscoring the need for chamber methods that minimize such
1069 artifacts. In contrast, our dynamic chamber system, with a chamber-specific λ correction and RC,
1070 enables robust, bias-corrected quantification of both low and episodic NH₃ fluxes, as well as clear
1071 partitioning of emission and dilution terms, even under highly variable field conditions. Overall,
1072 the combination of dual-chamber design with explicit λ correction in our method provides more
1073 accurate and robust quantification of soil NH₃ emissions than single-chamber, eddy covariance, or
1074 relaxed eddy accumulation techniques, particularly for short-term or low-flux events.

1075

1076 **4. Conclusions**

1077 In this work, we presented a dynamic chamber system for N_r flux measurements, developed for
1078 the first time through the modification of commercially available chambers by implementing two
1079 key changes: the use of PTFE fittings instead of original brass fittings and the installation of an
1080 inert PFA film, which retains their actinic transparency. These modifications provide a targeted
1081 methodology for other researchers to convert commercially available chambers into those capable
1082 of measuring N_r. The performance of these modifications was quantified through the rise and fall
1083 time constants of target gas concentrations, as well as a reduction in reactive losses. The time
1084 constants for the transfer of GHGs were not different from those of a theoretically inert gas and
1085 showed no change from the modifications. Improved transmission for the reactive and surface-
1086 active N_r species NO₂, HONO, and NH₃ targeted here ranged from 0.8 to 2.6 minutes. Further
1087 improvement for NH₃ might be obtained by integration of heated gas transfer lines between the
1088 chambers and gas analyzers. Similarly, a commercial chamber multiplexing unit with stainless
1089 steel valves and fittings replaced with PTFE and PFA, respectively, resulted in a 9–27% reduction
1090 in surface losses of N_r compounds.

1091 Only NO₂ showed reactive loss in the system, and the loss fraction in the chambers in their
1092 unmodified configurations was up to ~36%. Losses were reduced to the gas analyzer detection

1093 limits (<10%) with the same fluoropolymer modifications when atmospherically relevant NO₂ and
1094 RH mixtures were introduced. Lastly, O₃ loss was pervasive within chambers in both their
1095 modified and unmodified configurations at 35% and 45% respectively, demonstrating the
1096 necessity of the RC. It allows characterization of deposited surface film reactivity for O₃, especially
1097 when obtaining quality O₃ measurements is needed to account for the conversion of NO to NO₂
1098 during a sampling period. Taken together, the modified commercial system is capable of
1099 measuring dynamic soil fluxes of GHGs and N_r when MC and RC are deployed simultaneously.

1100 Proof of concept flux measurements using this N_r dynamic chamber system were conducted using
1101 real agricultural soil samples in the lab, with a single chamber, and during a pilot study in the field
1102 with a measurement-reference chamber pair. The lab soil emissions were found to be consistent
1103 with prior field reports in the literature for NO and HONO, with unexpected emissions of NO₂ also
1104 observed. Substantial variability in NO₂ and HONO emissions between replicates demonstrates
1105 the potential heterogeneity of soil emissions that may result from samples kept intact and subject
1106 to minimal preparation conditions. Upon the addition of typical fertilizers, like urea, substantial
1107 NH₃ and N₂O emissions fluxes matched expectations, with increasing quantities of NO, NO₂, and
1108 HONO as the soil water content decreased.

1109 Last, fully automated operation of the chambers was carried out in a field pilot study with the
1110 delivery of external fertilizer conducted at the midpoint of the two-week period to stimulate N_r
1111 emissions, mainly in the form of NH₃. Continuous flux observations were made by switching
1112 sample flows between the RC and MC with a custom-built valve system to obtain continuous N_r
1113 fluxes. While the details of the entire campaign will be presented in a future manuscript, it was
1114 shown here how the developed measurement technique yields reliable flux determinations by
1115 accounting for known reactions and our lab-derived surface effects. The mathematical foundation
1116 of each term and its error in a mass balance equation, which are central to reducing flux bias, are
1117 fully described. The observed fluxes from our dynamic chambers are simpler to quantify with
1118 standard gas analyzers and can be compared readily with prior reports in the literature from other
1119 common flux techniques. The duration of the chamber closure for the modified NO_x analyzer used
1120 in this work made a 30-minute observation necessary to obtain sufficient measurements for a
1121 reliable flux determination. Use of higher time resolution gas analyzers can readily reduce the
1122 observation period and continue to produce reliable fluxes, depending on the flux detection limit

1123 desired, and tolerance for inflated surface effects. One key limitation of the dynamic chamber
1124 approach is the limited footprint covered in a system that is notoriously heterogeneous, where eddy
1125 covariance and relaxed eddy accumulation flux approaches are less prone to this effect. Using a
1126 multiplexer and a larger array of dynamic chambers, it is possible to reduce the susceptibility of
1127 the dynamic chamber approach to this issue. One further limitation is that the chamber and gas
1128 transfer line surfaces may accumulate material and change the mass transfer of gases, particularly
1129 NH_3 , over time. This effect can be monitored using the reference chamber if sufficient quantities
1130 are present in the ambient air, via the dilution decay rate and characterized in situ by a standard
1131 addition of the necessary gases to the headspace.

1132 Through our modifications and validation, this work provides insight into how commercial
1133 dynamic chamber options, like those offered by Eosense, can be modified easily for scientists from
1134 various disciplines interested in studying N_r exchange at atmospheric interfaces. This is
1135 particularly important for research groups which currently do not have the expertise and resources
1136 to develop their own N_r flux measurement systems. The modified system utilizes destructive
1137 sampling techniques, as opposed to the re-circulation of chamber air, enabling integration of the
1138 dynamic chamber approach with various standard gas analysis instruments (e.g., NO_x
1139 chemiluminescence) to study their exchange. The large footprint allows gas concentrations to
1140 change in easily determined quantities even for very small fluxes. We show here, for the first time,
1141 that such a system can provide simultaneous measurement of NO , NO_2 , HONO , NH_3 , CO_2 , H_2O ,
1142 CH_4 , and N_2O fluxes. In addition, we show fully automated operation of the chambers, switching
1143 of sample flows, and data collection workflows for continuous and unattended measurements of
1144 fluxes at field sites. Ideally, modern instrumentation like the ToF-CIMS would be coupled with
1145 this system to shorten the chamber closure duration, and better distinguish HONO from other NO_y
1146 fluxes, instead of a modified NO_x analyzer. Given the pressing need to understand global
1147 perturbations to the biogeochemical cycle of N , reduce nitrogen use in agriculture, and gauge the
1148 impacts of N status on biodiversity or ecosystem function, wider accessibility of N_r flux techniques
1149 for the global research community is needed to increase the pace of research outcomes and improve
1150 the capacity for interdisciplinary work between atmospheric and earth system researchers.

1151

1152

1153 **Data Availability:** Data is available upon request from the Corresponding Author.

1154 **Competing Interests:** TCV received supporting in-kind funds for this work from Eosense, Inc.
1155 and Picarro as it is mandatory in the NSERC Alliance Missions programme funding structure
1156 which facilitates research partnerships between the academy and industry. NN, CC, and SE are
1157 employed by Eosense, Inc.

1158 **Author contributions:** TCV designed and oversaw the experiments, acquired funding, wrote parts
1159 of the manuscript, and guided writing and revision of all sections of the manuscript. MS wrote the
1160 manuscript and performed all the lab experiments. KZA carried out the multiplexer experiments,
1161 conducted data analysis for the fill-empty experiment, provided guidance and feedback on the
1162 derivation of the mass balance flux model, and assisted in the revision of the manuscript. DF
1163 conducted some of the field measurements, worked up the pilot field study results and derived the
1164 dual chamber mass balance flux calculations, and made contributions to the writing and revision
1165 of the manuscript. LRC helped design the experiments, modify the chambers, write the LabVIEW
1166 code, conduct the pilot field measurements, and contributed to manuscript preparation and
1167 revision. AM contributed to the initial chamber lab setup and revision of the manuscript. FS
1168 performed some fill-empty and NO₂ loss experiments, designed the custom valve switching
1169 system, modified LabVIEW code for the pilot field measurements, and contributed to initial drafts
1170 of the manuscript. YEI and TH assisted with the GHG fill-empty experiments, YEI supported the
1171 pilot field study, and both contributed to manuscript revision. NN, CC, and SE provided technical
1172 support with setting up and modifying the chambers and multiplexer.

1173 **Acknowledgements:** We gratefully acknowledge the support of Picarro for facilitating use of the
1174 G2509 analyzer during the chamber characterizations, lab experiments, and pilot study
1175 components of this work. The team at Shawnasey Farms Ltd. provided access to storage and
1176 machinery to install the experimental agricultural site for the pilot project, helped with daily
1177 campaign logistics, and the collection of soil samples.

1178 **Financial Support:** All components of this work were supported by funding to TCV by the
1179 Natural Sciences and Engineering Research Council (NSERC) Alliance Missions program
1180 (ALLRP 570577-2021), with additional support from the NSERC Discovery Grants and Early
1181 Career Launch programmes (RGPIN-2020-06166 and DGEGR-2020-00186). MS and YEI were

1182 supported by Ontario Graduate Scholarships, and MS was further supported by a Charles Hantho
1183 Award in Atmospheric Chemistry and the Enbridge Graduate Student Award.

1184

1185 **5. References**

- 1186 Almand-Hunter, B. B., Walker, J. T., Masson, N. P., Hafford, L., & Hannigan, M. P. (2015).
1187 Development and validation of inexpensive, automated, dynamic flux chambers.
1188 *Atmospheric Measurement Techniques*, 8(1), 267–280. [https://doi.org/10.5194/amt-8-267-](https://doi.org/10.5194/amt-8-267-2015)
1189 [2015](https://doi.org/10.5194/amt-8-267-2015)
- 1190 Anas, M., Liao, F., Verma, K. K., Sarwar, M. A., Mahmood, A., Chen, Z. L., Li, Q., Zeng, X. P.,
1191 Liu, Y., & Li, Y. R. (2020). Fate of nitrogen in agriculture and environment: agronomic,
1192 eco-physiological and molecular approaches to improve nitrogen use efficiency. In
1193 *Biological Research* (Vol. 53, Issue 1). BioMed Central Ltd.
1194 <https://doi.org/10.1186/s40659-020-00312-4>
- 1195 Aneja, V. P., Blunden, J., Claiborn, C. S., & Rogers, H. H. (2006). Dynamic Chamber System to
1196 Measure Gaseous Compounds Emissions and Atmospheric-Biospheric Interactions.
1197 *Environmental Simulation Chambers: Application to Atmospheric Chemical Processes*, 97–
1198 109. https://doi.org/10.1007/1-4020-4232-9_7
- 1199 Anthony, T. L., & Silver, W. L. (2024). Hot spots and hot moments of greenhouse gas emissions
1200 in agricultural peatlands. *Biogeochemistry*, 167(4), 461–477.
1201 <https://doi.org/10.1007/s10533-023-01095-y>
- 1202 Bao, F., Cheng, Y., Kuhn, U., Li, G., Wang, W., Kratz, A. M., Weber, J., Weber, B., Pöschl, U.,
1203 & Su, H. (2022). Key Role of Equilibrium HONO Concentration over Soil in Quantifying
1204 Soil–Atmosphere HONO Fluxes. *Environmental Science & Technology*.
1205 <https://doi.org/10.1021/acs.est.1c06716>
- 1206 Barney, W. S., & Finlayson-Pitts, B. J. (2000). Enhancement of N₂O₄ on Porous Glass at Room
1207 Temperature: A Key Intermediate in the Heterogeneous Hydrolysis of NO₂? *Journal of*
1208 *Physical Chemistry A*, 104(2), 171–175. <https://doi.org/10.1021/jp993169b>
- 1209 Becciolini, V., Leso, L., Fuertes Gimeno, E., Rossi, G., Barbari, M., Dalla Marta, A., Orlandini,
1210 S., & Verdi, L. (2024). Nitrogen loss abatement from dairy cow excreta through urine and
1211 faeces separation: The effect of temperature and exposure period on NH₃ fluxes.
1212 *Agricultural Systems*, 216. <https://doi.org/10.1016/j.agry.2024.103898>
- 1213 Behera, S. N., Sharma, M., Aneja, V. P., & Balasubramanian, R. (2013). Ammonia in the
1214 atmosphere: A review on emission sources, atmospheric chemistry and deposition on
1215 terrestrial bodies. In *Environmental Science and Pollution Research* (Vol. 20, Issue 11, pp.
1216 8092–8131). <https://doi.org/10.1007/s11356-013-2051-9>
- 1217 Behrendt, T., Veres, P. R., Ashuri, F., Song, G., Flanz, M., Mamtimin, B., Bruse, M., Williams,
1218 J., & Meixner, F. X. (2014). Characterisation of NO production and consumption: New
1219 insights by an improved laboratory dynamic chamber technique. *Biogeosciences*, 11(19),
1220 5463–5492. <https://doi.org/10.5194/bg-11-5463-2014>
- 1221 Benedict, K. B., Prenni, A. J., Carrico, C. M., Sullivan, A. P., Schichtel, B. A., & Collett, J. L.
1222 (2017). Enhanced concentrations of reactive nitrogen species in wildfire smoke.
1223 *Atmospheric Environment*, 148, 8–15. <https://doi.org/10.1016/j.atmosenv.2016.10.030>
- 1224 Burkholder, J. B., Cox, R. A., & Ravishankara, A. R. (2015). Atmospheric Degradation of Ozone
1225 Depleting Substances, Their Substitutes, and Related Species. *Chemical Reviews*, 115(10),
1226 3704–3759. <https://doi.org/10.1021/cr5006759>

1227 Butterbach-Bahl, K., & Dannenmann, M. (2011). Denitrification and associated soil N₂O
1228 emissions due to agricultural activities in a changing climate. *Current Opinion in*
1229 *Environmental Sustainability*, 3(5), 389–395. <https://doi.org/10.1016/j.cosust.2011.08.004>

1230 Chiaravalloti, I., Theunissen, N., Zhang, S., Wang, J., Sun, F., Ahmed, A. A., Pihlap, E.,
1231 Reinhard, C. T., & Planavsky, N. J. (2023). Mitigation of soil nitrous oxide emissions
1232 during maize production with basalt amendments. *Frontiers in Climate*, 5.
1233 <https://doi.org/10.3389/fclim.2023.1203043>

1234 Crilley, L. R., Kramer, L. J., Ouyang, B., Duan, J., Zhang, W., Tong, S., Ge, M., Tang, K., Qin,
1235 M., Xe, P., Shaw, M. D., Lewis, A. C., Mehra, A., Bannan, T. J., Worrall, S. D., Priestley,
1236 M., Bacak, A., Coe, H., Allan, J., ... Bloss, W. J. (2019). *Intercomparison of nitrous acid*
1237 *(HONO) measurement techniques in a megacity (Beijing)*. [https://doi.org/10.5194/amt-](https://doi.org/10.5194/amt-2019-139)
1238 [2019-139](https://doi.org/10.5194/amt-2019-139)

1239 Crilley, L. R., Lao, M., Salehpoor, L., & VandenBoer, T. C. (2023). Emerging investigator
1240 series: an instrument to measure and speciate the total reactive nitrogen budget indoors:
1241 description and field measurements. *Environmental Science: Processes and Impacts*, 25(3),
1242 389–404. <https://doi.org/10.1039/d2em00446a>

1243 Degaspari, I. A. M., Soares, J. R., Montezano, Z. F., Del Grosso, S. J., Vitti, A. C., Rossetto, R.,
1244 & Cantarella, H. (2020). Nitrogen sources and application rates affect emissions of N₂O
1245 and NH₃ in sugarcane. *Nutrient Cycling in Agroecosystems*, 116(3), 329–344.
1246 <https://doi.org/10.1007/s10705-019-10045-w>

1247 Delaria, E. R., & Cohen, R. C. (2023). Measurements of Atmosphere-Biosphere Exchange of
1248 Oxidized Nitrogen and Implications for the Chemistry of Atmospheric NO_x. *Accounts of*
1249 *Chemical Research*, 56(13), 1720–1730. <https://doi.org/10.1021/acs.accounts.3c00090>

1250 Dennis, R. L., Mathur, R., Pleim, J. E., & Walker, J. T. (2010). Fate of ammonia emissions at the
1251 local to regional scale as simulated by the Community Multiscale Air Quality model.
1252 *Atmospheric Pollution Research*, 1(4), 207–214. <https://doi.org/10.5094/APR.2010.027>

1253 Ebnesajjad, S. (2017). Introduction to Fluoropolymers. *Applied Plastics Engineering Handbook:*
1254 *Processing, Materials, and Applications: Second Edition*, 55–71.
1255 <https://doi.org/10.1016/B978-0-323-39040-8.00003-1>

1256 Edwards, T. M., Puglis, H. J., Kent, D. B., Durán, J. L., Bradshaw, L. M., & Farag, A. M.
1257 (2024). Ammonia and aquatic ecosystems – A review of global sources, biogeochemical
1258 cycling, and effects on fish. In *Science of the Total Environment* (Vol. 907). Elsevier B.V.
1259 <https://doi.org/10.1016/j.scitotenv.2023.167911>

1260 Ellis, R. A., Murphy, J. G., Pattey, E., Van Haarlem, R., O'Brien, J. M., & Herndon, S. C.
1261 (2010). Characterizing a Quantum Cascade Tunable Infrared Laser Differential Absorption
1262 Spectrometer (QC-TILDAS) for measurements of atmospheric ammonia. *Atmospheric*
1263 *Measurement Techniques*, 3(2), 397–406. <https://doi.org/10.5194/amt-3-397-2010>

1264 Finlayson-Pitts, B. J., Wingen, L. M., Sumner, A. L., Syomin, D., & Ramazan, K. A. (2003). The
1265 heterogeneous hydrolysis of NO₂ in laboratory systems and in outdoor and indoor
1266 atmospheres: An integrated mechanism. *Physical Chemistry Chemical Physics*, 5(2), 223–
1267 242. <https://doi.org/10.1039/b208564j>

1268 Fowler, D., Coyle, M., Skiba, U., Sutton, M. A., Cape, J. N., Reis, S., Sheppard, L. J., Jenkins,
1269 A., Grizzetti, B., Galloway, J. N., Vitousek, P., Leach, A., Bouwman, A. F., Butterbach-
1270 Bahl, K., Dentener, F., Stevenson, D., Amann, M., & Voss, M. (2013). The global nitrogen
1271 cycle in the twenty-first century. *Philosophical Transactions of the Royal Society B:*
1272 *Biological Sciences*, 368(1621). <https://doi.org/10.1098/rstb.2013.0164>

1273 Geddes, J. A., & Murphy, J. G. (2014). Observations of reactive nitrogen oxide fluxes by eddy
1274 covariance above two midlatitude North American mixed hardwood forests. *Atmospheric*
1275 *Chemistry and Physics*, 14(6), 2939–2957. <https://doi.org/10.5194/acp-14-2939-2014>

1276 George, C., Ammann, M., D’Anna, B., Donaldson, D. J., & Nizkorodov, S. A. (2015).
1277 Heterogeneous Photochemistry in the Atmosphere. *Chemical Reviews*, 115(10), 4218–4258.
1278 <https://doi.org/10.1021/cr500648z>

1279 Gong, C., Wang, Y., Tian, H., Kou-Giesbrecht, S., Vuichard, N., & Zaehle, S. (2025).
1280 Uncertainties in fertilizer-induced emissions of soil nitrogen oxide and the associated
1281 impacts on ground-level ozone and methane. *EGUsphere*.
1282 <https://doi.org/10.5194/egusphere-2025-1416>

1283 González Ortiz, Alberto., Guerreiro, Cristina., & Soares, Joana. (2020). *Air quality in Europe:*
1284 *2020 report*. European Environment Agency. <https://doi.org/10.2800/786656>

1285 Govoni Brondi, M., Bortoletto-Santos, R., Farias, J. G., Farinas, C. S., Ammar, M., Ribeiro, C.,
1286 Williams, C., & Baltrusaitis, J. (2024). Mechanochemically Synthesized Nitrogen-Efficient
1287 Mg- and Zn-Ammonium Carbonate Fertilizers. *ACS Sustainable Chemistry and*
1288 *Engineering*, 12(16), 6182–6193. <https://doi.org/10.1021/acssuschemeng.3c07785>

1289 Ha, P. T. M., Kanaya, Y., Taketani, F., Andres Hernandez, M. D., Schreiner, B., Pfeilsticker, K.,
1290 & Sudo, K. (2023). Implementation of HONO into the chemistry-climate model CHASER
1291 (V4.0): Roles in tropospheric chemistry. *Geoscientific Model Development*, 16(3), 927–960.
1292 <https://doi.org/10.5194/gmd-16-927-2023>

1293 He, Y., Zhou, X., Hou, J., Gao, H., & Bertman, S. B. (2006). Importance of dew in controlling
1294 the air-surface exchange of HONO in rural forested environments. *Geophysical Research*
1295 *Letters*, 33(2). <https://doi.org/10.1029/2005GL024348>

1296 Huang, G., Zhou, X., Deng, G., Qiao, H., & Civerolo, K. (2002). Measurements of atmospheric
1297 nitrous acid and nitric acid. *Atmospheric Environment*, 36(13), 2225–2235.
1298 [https://doi.org/10.1016/S1352-2310\(02\)00170-X](https://doi.org/10.1016/S1352-2310(02)00170-X)

1299 Huber, D. E., Kort, E. A., & Steiner, A. L. (2024). Soil Moisture, Soil NO_x and Regional Air
1300 Quality in the Agricultural Central United States. *Journal of Geophysical Research:*
1301 *Atmospheres*, 129(12). <https://doi.org/10.1029/2024JD041015>

1302 IPCC. (2023). *Climate Change 2021- The Physical Science Basis*. Cambridge University Press.
1303 <https://doi.org/https://doi.org/10.1017/9781009157896>

1304 Jang, J.-H., Hong, J., Kim, J. B., Park, S., Hwang, K., Kim, J., Kim, J. Y., Bae, G.-N., Kim, S., &
1305 Kim, K. H. (2025). Influence of atmospheric ammonia on secondary inorganic aerosol
1306 formation in PM_{2.5} during spring 2024 in the Hongseong area, Republic of Korea.
1307 *Atmospheric Environment*, 121363. <https://doi.org/10.1016/j.atmosenv.2025.121363>

1308 Kamboures, M. A., Raff, J. D., Miller, Y., Phillips, L. F., Finlayson-Pitts, B. J., & Gerber, R. B.
1309 (2008). Complexes of HNO₃ and NO₃- with NO₂ and N₂O₄, and their potential role in

1310 atmospheric HONO formation. *Physical Chemistry Chemical Physics*, 10(39), 6019–6032.
1311 <https://doi.org/10.1039/b805330h>

1312 Kamp, J. N., Häni, C., Nyord, T., Feilberg, A., & Sørensen, L. L. (2020). The aerodynamic
1313 gradient method: Implications of non-simultaneous measurements at alternating heights.
1314 *Atmosphere*, 11(10). <https://doi.org/10.3390/atmos11101067>

1315 Kleffmann, J., Gavriloaiei, T., Hofzumahaus, A., Holland, F., Koppmann, R., Rupp, L.,
1316 Schlosser, E., Siese, M., & Wahner, A. (2005). Daytime formation of nitrous acid: A major
1317 source of OH radicals in a forest. *Geophysical Research Letters*, 32(5), 1–4.
1318 <https://doi.org/10.1029/2005GL022524>

1319 Kolari, P., Bäck, J., Taipale, R., Ruuskanen, T. M., Kajos, M. K., Rinne, J., Kulmala, M., &
1320 Hari, P. (2012). Evaluation of accuracy in measurements of VOC emissions with dynamic
1321 chamber system. *Atmospheric Environment*, 62, 344–351.
1322 <https://doi.org/10.1016/j.atmosenv.2012.08.054>

1323 Kool, D. M., Wrage, N., Zechmeister-Boltenstern, S., Pfeffer, M., Brus, D., Oenema, O., & Van
1324 Groenigen, J. W. (2010). Nitrifier denitrification can be a source of N₂O from soil: A
1325 revised approach to the dual-isotope labelling method. *European Journal of Soil Science*,
1326 61(5), 759–772. <https://doi.org/10.1111/j.1365-2389.2010.01270.x>

1327 Lao, M., Crilley, L. R., Salehpoor, L., Furlani, T. C., Bourgeois, I., Andrew Neuman, J., Rollins,
1328 A. W., Veres, P. R., Washenfelder, R. A., Womack, C. C., Young, C. J., & VandenBoer, T.
1329 C. (2020). A portable, robust, stable, and tunable calibration source for gas-phase nitrous
1330 acid (HONO). *Atmospheric Measurement Techniques*, 13(11), 5873–5890.
1331 <https://doi.org/10.5194/amt-13-5873-2020>

1332 Laufs, S., Cazaunau, M., Stella, P., Kurtenbach, R., Cellier, P., Mellouki, A., Loubet, B., &
1333 Kleffmann, J. (2017). Diurnal fluxes of HONO above a crop rotation. *Atmospheric
1334 Chemistry and Physics*, 17(11), 6907–6923. <https://doi.org/10.5194/acp-17-6907-2017>

1335 Lee, B. H., Lopez-Hilfiker, F. D., Mohr, C., Kurtén, T., Worsnop, D. R., & Thornton, J. A.
1336 (2014). An iodide-adduct high-resolution time-of-flight chemical-ionization mass
1337 spectrometer: Application to atmospheric inorganic and organic compounds. *Environmental
1338 Science and Technology*, 48(11), 6309–6317. <https://doi.org/10.1021/es500362a>

1339 Lehnert, N., Musselman, B. W., Seefeldt, L. C., & Gutenberg-university, J. (2021). Grand
1340 Challenges in the nitrogen cycle. *Chemical Society Reviews*, 50, 3640–3646.
1341 <https://doi.org/10.1039/d0cs00923g>

1342 Li, L., Fan, W., Kang, X., Wang, Y., Cui, X., Xu, C., Griffin, K. L., & Hao, Y. (2016).
1343 Responses of greenhouse gas fluxes to climate extremes in a semiarid grassland.
1344 *Atmospheric Environment*, 142, 32–42. <https://doi.org/10.1016/j.atmosenv.2016.07.039>

1345 Lipiec, J., Walczak, R., Witkowska-Walczak, B., Nosalewicz, A., Słowińska-Jurkiewicz, A., &
1346 Sławiński, C. (2007). The effect of aggregate size on water retention and pore structure of
1347 two silt loam soils of different genesis. *Soil and Tillage Research*, 97(2), 239–246.
1348 <https://doi.org/10.1016/j.still.2007.10.001>

1349 Liu, L., Zhang, X., Xu, W., Liu, X., Li, Y., Wei, J., Wang, Z., & Lu, X. (2020). Ammonia
1350 volatilization as the major nitrogen loss pathway in dryland agro-ecosystems.
1351 *Environmental Pollution*, 265. <https://doi.org/10.1016/j.envpol.2020.114862>

- 1352 Liu, Zheng, X., Li, Y., Yu, J., Ding, H., Sveen, T. R., & Zhang, Y. (2022). Soil moisture
1353 determines nitrous oxide emission and uptake. *Science of the Total Environment*, 822.
1354 <https://doi.org/10.1016/j.scitotenv.2022.153566>
- 1355 Ludwig, J., Meixner, F. X., Vogel, B., & Forstner, J. (2001). Soil-air exchange of nitric oxide:
1356 An overview of processes, environmental factors, and modeling studies. *Biogeochemistry*,
1357 52(3), 225–257. <https://doi.org/10.1023/A:1006424330555>
- 1358 Luo, X., Zhang, M., Ni, Y., & Shen, G. (2025). Mitigation strategies for NH₃ and N₂O emissions
1359 in greenhouse agriculture: Insights into fertilizer management and nitrogen emission
1360 mechanisms. *Environmental Technology and Innovation*, 37.
1361 <https://doi.org/10.1016/j.eti.2024.103995>
- 1362 Maggiotto, S. R., Webb, J. A., & Thurtell, G. W. (2000). Nitrous and Nitrogen Oxide Emissions
1363 from Turfgrass Receiving Different Forms of Nitrogen Fertilizer. *American Society of*
1364 *Agronomy, Crop Science Society of America, and Soil Science Society of America*, 29, 621–
1365 630.
- 1366 Manco, A., Giaccone, M., Vitale, L., Maglione, G., Riccardi, M., Matteo, B. Di, Esposito, A.,
1367 Magliulo, V., & Tedeschi, A. (2025). Comparative Effects of Nitrogen Fertigation and
1368 Granular Fertilizer Application on Pepper Yield and Soil GHGs Emissions. *Horticulturae*,
1369 11(6). <https://doi.org/10.3390/horticulturae11060708>
- 1370 Mangalassery, S., Sjögersten, S., Sparkes, D. L., Sturrock, C. J., & Mooney, S. J. (2013). The
1371 effect of soil aggregate size on pore structure and its consequence on emission of
1372 greenhouse gases. *Soil and Tillage Research*, 132, 39–46.
1373 <https://doi.org/10.1016/j.still.2013.05.003>
- 1374 Meusel, H., Tamm, A., Kuhn, U., Wu, D., Lena Leifke, A., Fiedler, S., Ruckteschler, N.,
1375 Yordanova, P., Lang-Yona, N., Pöhlker, M., Lelieveld, J., Hoffmann, T., Pöschl, U., Su, H.,
1376 Weber, B., & Cheng, Y. (2018). Emission of nitrous acid from soil and biological soil crusts
1377 represents an important source of HONO in the remote atmosphere in Cyprus. *Atmospheric*
1378 *Chemistry and Physics*, 18(2), 799–813. <https://doi.org/10.5194/acp-18-799-2018>
- 1379 Min, K. E., Pusede, S. E., Browne, E. C., LaFranchi, B. W., & Cohen, R. C. (2014). Eddy
1380 covariance fluxes and vertical concentration gradient measurements of NO and NO₂ over a
1381 ponderosa pine ecosystem: Observational evidence for within-canopy chemical removal of
1382 NO_x. *Atmospheric Chemistry and Physics*, 14(11), 5495–5512. [https://doi.org/10.5194/acp-](https://doi.org/10.5194/acp-14-5495-2014)
1383 [14-5495-2014](https://doi.org/10.5194/acp-14-5495-2014)
- 1384 Mochizuki, T., Amagai, T., & Tani, A. (2018). Effects of soil water content and elevated CO₂
1385 concentration on the monoterpene emission rate of *Cryptomeria japonica*. *Science of the*
1386 *Total Environment*, 634, 900–908. <https://doi.org/10.1016/j.scitotenv.2018.04.025>
- 1387 Moravek, A., Foken, T., & Trebs, I. (2014). Application of a GC-ECD for measurements of
1388 biosphere-atmosphere exchange fluxes of peroxyacetyl nitrate using the relaxed eddy
1389 accumulation and gradient method. *Atmospheric Measurement Techniques*, 7(7), 2097–
1390 2119. <https://doi.org/10.5194/amt-7-2097-2014>
- 1391 Moravek, A., Singh, S., Pattey, E., Pelletier, L., & Murphy, J. G. (2019). Measurements and
1392 quality control of ammonia eddy covariance fluxes: A new strategy for high-frequency
1393 attenuation correction. *Atmospheric Measurement Techniques*, 12(11), 6059–6078.
1394 <https://doi.org/10.5194/amt-12-6059-2019>

1395 Mosier, A. R. (2008). Exchange of Gaseous Nitrogen Compounds Between Terrestrial Systems
1396 and the Atmosphere. *Nitrogen in the Environment*, 443–462. [https://doi.org/10.1016/B978-](https://doi.org/10.1016/B978-0-12-374347-3.00013-5)
1397 [0-12-374347-3.00013-5](https://doi.org/10.1016/B978-0-12-374347-3.00013-5)

1398 Mushinski, R. M., Phillips, R. P., Payne, Z. C., Abney, R. B., Jo, I., Fei, S., Pusede, S. E., White,
1399 J. R., Rusch, D. B., & Raff, J. D. (2019). Microbial mechanisms and ecosystem flux
1400 estimation for aerobic NO_y emissions from deciduous forest soils. *Proceedings of the*
1401 *National Academy of Sciences of the United States of America*, 116(6), 2138–2145.
1402 <https://doi.org/10.1073/pnas.1814632116>

1403 Neuman, J. A., Trainer, M., Brown, S. S., Min, K. E., Nowak, J. B., Parrish, D. D., Peischl, J.,
1404 Pollack, I. B., Roberts, J. M., Ryerson, T. B., & Veres, P. R. (2016). HONO emission and
1405 production determined from airborne measurements over the Southeast U.S. *Journal of*
1406 *Geophysical Research*, 121(15), 9237–9250. <https://doi.org/10.1002/2016JD025197>

1407 Nodeh-Farahani, D., Bentley, J. N., Crilley, L. R., Caputo, C. B., & VandenBoer, T. C. (2021). A
1408 boron dipyrromethene (BODIPY) based probe for selective passive sampling of
1409 atmospheric nitrous acid (HONO) indoors. *Analyst*, 146(18), 5756–5766.
1410 <https://doi.org/10.1039/d1an01089a>

1411 Okiti, I., Efakwu, G., Pindus, M., & Kasak, K. (2025). Environmental and biogeochemical
1412 drivers of CH₄ and N₂O flux variability in treatment wetlands. *Ecological Engineering*,
1413 219. <https://doi.org/10.1016/j.ecoleng.2025.107705>

1414 Oswald, R., Behrendt, T., Ermel, M., Wu, D., Su, H., Cheng, Y., Breuninger, C., Moravek, A.,
1415 Mougín, E., Delon, C., Loubet, B., Pommerening-Röser, A., Sörgel, M., Pöschl, U.,
1416 Hoffmann, T., Andreae, M. O., Meixner, F. X., & Trebs, I. (2013). HONO emissions from
1417 soil bacteria as a major source of atmospheric reactive nitrogen. *Science*, 341(6151), 1233–
1418 1235. <https://doi.org/10.1126/science.1242266>

1419 Pan, B., Lam, S. K., Mosier, A., Luo, Y., & Chen, D. (2016). Ammonia volatilization from
1420 synthetic fertilizers and its mitigation strategies: A global synthesis. *Agriculture,*
1421 *Ecosystems and Environment*, 232, 283–289. <https://doi.org/10.1016/j.agee.2016.08.019>

1422 Pan, B., Xia, L., Lam, S. K., Wang, E., Zhang, Y., Mosier, A., & Chen, D. (2022). A global
1423 synthesis of soil denitrification: Driving factors and mitigation strategies. *Agriculture,*
1424 *Ecosystems and Environment*, 327(September 2021), 107850.
1425 <https://doi.org/10.1016/j.agee.2021.107850>

1426 Pape, L., Ammann, C., Nyfeler-Brunner, A., Spirig, C., Hens, K., & Meixner, F. X. (2009). An
1427 automated dynamic chamber system for surface exchange measurement of non-reactive and
1428 reactive trace gases of grassland ecosystems. *Biogeosciences*, 6(3), 405–429.
1429 <https://doi.org/10.5194/bg-6-405-2009>

1430 Paulot, F., Jacob, D. J., Pinder, R. W., Bash, J. O., Travis, K., & Henze, D. K. (2014). Ammonia
1431 emissions in the United States, European Union, and China derived by high-resolution
1432 inversion of ammonium wet deposition data: Interpretation with a new agricultural
1433 emissions inventory (MASAGE_NH₃). *Journal of Geophysical Research*, 119(7), 4343–
1434 4364. <https://doi.org/10.1002/2013JD021130>

1435 Plake, D., Sörgel, M., Stella, P., Held, A., & Trebs, I. (2015). Influence of meteorology and
1436 anthropogenic pollution on chemical flux divergence of the NO-NO₂-O₃ triad above and

1437 within a natural grassland canopy. *Biogeosciences*, 12(4), 945–959.
1438 <https://doi.org/10.5194/bg-12-945-2015>

1439 Plake, D., Stella, P., Moravek, A., Mayer, J. C., Ammann, C., Held, A., & Trebs, I. (2015).
1440 Comparison of ozone deposition measured with the dynamic chamber and the eddy
1441 covariance method. *Agricultural and Forest Meteorology*, 206, 97–112.
1442 <https://doi.org/10.1016/j.agrformet.2015.02.014>

1443 Possanzini, M., Febo, A., & Liberti, A. (1983). New design of a high-performance denuder for
1444 the sampling of atmospheric pollutants. *Atmospheric Environment (1967)*, 17(12), 2605–
1445 2610. [https://doi.org/10.1016/0004-6981\(83\)90089-6](https://doi.org/10.1016/0004-6981(83)90089-6)

1446 Pugliese, G., Ingrisch, J., Meredith, L. K., Pfannerstill, E. Y., Klüpfel, T., Meeran, K. Byron, J.,
1447 Purser, G. Gil-Loaiza, J., van Haren, J., Dontsova, K., Kreuzwieser, J., Ladd, S. N., Werner,
1448 C. & Williams, J. (2023). Effects of drought and recovery on soil volatile organic
1449 compound fluxes in an experimental forest. *Nature Communications*, 14:5064.
1450 <https://doi.org/10.1038/s41467-023-40661-8>

1451 Purchase, M. L., Bending, G. D., & Mushinski, R. M. (2023). Spatiotemporal Variations of Soil
1452 Reactive Nitrogen Oxide Fluxes across the Anthropogenic Landscape. *Environmental
1453 Science and Technology*, 57(43), 16348–16360. <https://doi.org/10.1021/acs.est.3c05849>

1454 Ramazan, K. A., Syomin, D., & Finlayson-Pitts, B. J. (2004). The photochemical production of
1455 HONO during the heterogeneous hydrolysis of NO₂. *Physical Chemistry Chemical Physics*,
1456 6(14), 3836–3843. <https://doi.org/10.1039/b402195a>

1457 Reed, C., Brumby, C. A., Crilley, L. R., Kramer, L. J., Bloss, W. J., Seakins, P. W., Lee, J. D., &
1458 Carpenter, L. J. (2016). HONO measurement by differential photolysis. *Atmospheric
1459 Measurement Techniques*, 9(6), 2483–2495. <https://doi.org/10.5194/amt-9-2483-2016>

1460 Ren, X., Sanders, J. E., Rajendran, A., Weber, R. J., Goldstein, A. H., Pusede, S. E., Browne, E.
1461 C., Min, K. E., & Cohen, R. C. (2011). A relaxed eddy accumulation system for measuring
1462 vertical fluxes of nitrous acid. *Atmospheric Measurement Techniques*, 4(10), 2093–2103.
1463 <https://doi.org/10.5194/amt-4-2093-2011>

1464 Ren, Y., Stieger, B., Spindler, G., Grosselin, B., Mellouki, A., Tuch, T., Wiedensohler, A., &
1465 Herrmann, H. (2020). Role of the dew water on the ground surface in HONO distribution: A
1466 case measurement in Melpitz. *Atmospheric Chemistry and Physics*, 20(21), 13069–13089.
1467 <https://doi.org/10.5194/acp-20-13069-2020>

1468 Richardson, K., Steffen, W., Lucht, W., Bendtsen, J., Cornell, S. E., Donges, J. F., Drüke, M.,
1469 Fetzer, I., Bala, G., Von Bloh, W., Feulner, G., Fiedler, S., Gerten, D., Gleeson, T.,
1470 Hofmann, M., Huiskamp, W., Kummu, M., Mohan, C., Nogués-Bravo, D., ... Rockström, J.
1471 (2023). *Earth beyond six of nine planetary boundaries*. <https://www.science.org>

1472 Scharko, N. K., Schu, U. M. E., Berke, A. E., Banina, L., Peel, H. R., Donaldson, M. A.,
1473 Hemmerich, C., White, R., & Ra, J. D. (2015). *Combined Flux Chamber and Genomics
1474 Approach Links Nitrous Acid Emissions to Ammonia Oxidizing Bacteria and Archaea in
1475 Urban and Agricultural Soil*. <https://doi.org/10.1021/acs.est.5b00838>

1476 Schindlbacher, A., Zechmeister-Boltenstern, S., & Jandl, R. (2009). Carbon losses due to soil
1477 warming: Do autotrophic and heterotrophic soil respiration respond equally? *Global
1478 Change Biology*, 15(4), 901–913. <https://doi.org/10.1111/j.1365-2486.2008.01757.x>

- 1479 Schlesinger, W. H. (2020). *Biogeochemistry: An Analysis of Global Change* (4th ed.). Academic
 1480 Press. <https://doi.org/https://doi.org/10.1016/C2018-0-03255-3>
- 1481 Seinfeld, J. H., & Pandis, S. N. (2006). *Atmospheric chemistry and physics: from air pollution to*
 1482 *climate change*. (2nd edition). John Wiley & Sons.
- 1483 Shah, S. B., Grabow, G. L., & Westerman, P. W. (2006). *Ammonia adsorption in five types of*
 1484 *flexible tubing materials*. <https://doi.org/10.13031/2013.22253>
- 1485 Song, Y., Xue, C., Zhang, Y., Liu, P., Bao, F., Li, X., & Mu, Y. (2023). *Measurement Report:*
 1486 *Exchange Fluxes of HONO over Agricultural Fields in the North China Plain. July, 1–38.*
 1487 <https://zenodo.org/record/8115973>
- 1488 Sörgel, M., Trebs, I., Wu, D., & Held, A. (2015). A comparison of measured HONO uptake and
 1489 release with calculated source strengths in a heterogeneous forest environment. *Atmospheric*
 1490 *Chemistry and Physics*, 15(16), 9237–9251. <https://doi.org/10.5194/acp-15-9237-2015>
- 1491 Spataro, F., & Ianniello, A. (2014). Sources of atmospheric nitrous acid: State of the science,
 1492 current research needs, and future prospects. *Journal of the Air and Waste Management*
 1493 *Association*, 64(11), 1232–1250. <https://doi.org/10.1080/10962247.2014.952846>
- 1494 Stepniewski, W., Stepniewska, Z., & Rozej, A. (2015). Gas Exchange in Soils. *Soil*
 1495 *Management: Building a Stable Base for Agriculture*, 117–144.
 1496 <https://doi.org/10.2136/2011.soilmanagement.c8>
- 1497 Su, H., Cheng, Y., Oswald, R., Behrendt, T., Trebs, I., Meixner, F. X., Andreae, M. O., Cheng,
 1498 P., Zhang, Y., & Pöschl, U. (2011). Soil nitrite as a source of atmospheric HONO and OH
 1499 radicals. *Science*, 333(6049), 1616–1618. <https://doi.org/10.1126/science.1207687>
- 1500 Tang, K., Qin, M., Duan, J., Fang, W., Meng, F., Liang, S., Xie, P., Liu, J., Liu, W., Xue, C., &
 1501 Mu, Y. (2019). A dual dynamic chamber system based on IBBCEAS for measuring fluxes
 1502 of nitrous acid in agricultural fields in the North China Plain. *Atmospheric Environment*,
 1503 196(May 2018), 10–19. <https://doi.org/10.1016/j.atmosenv.2018.09.059>
- 1504 Tang, K., Qin, M., Fang, W., Duan, J., Meng, F., Ye, K., Zhang, H., Xie, P., Liu, J., Liu, W.,
 1505 Feng, Y., Huang, Y., & Ni, T. (2020). An automated dynamic chamber system for exchange
 1506 flux measurement of reactive nitrogen oxides (HONO and NOX) in farmland ecosystems of
 1507 the Huaihe River Basin, China. *Science of the Total Environment*, 745(X), 140867.
 1508 <https://doi.org/10.1016/j.scitotenv.2020.140867>
- 1509 Tian, H., Pan, N., Thompson, R. L., Canadell, J. G., Suntharalingam, P., Regnier, P., Davidson,
 1510 E. A., Prather, M., Ciais, P., Muntean, M., Pan, S., Winiwarter, W., Zaehle, S., Zhou, F.,
 1511 Jackson, R. B., Bange, H. W., Berthet, S., Bian, Z., Bianchi, D., ... Zhu, Q. (2024). Global
 1512 nitrous oxide budget (1980-2020). *Earth System Science Data*, 16(6), 2543–2604.
 1513 <https://doi.org/10.5194/essd-16-2543-2024>
- 1514 Vaaitinen, O., Metsälä, M., Persijn, S., Vainio, M., & Halonen, L. (2014). Adsorption of
 1515 ammonia on treated stainless steel and polymer surfaces. *Applied Physics B: Lasers and*
 1516 *Optics*, 115(2), 185–196. <https://doi.org/10.1007/s00340-013-5590-3>
- 1517 VandenBoer, T. C., Brown, S. S., Murphy, J. G., Keene, W. C., Young, C. J., Pszenny, A. A. P.
 1518 P., Kim, S., Warneke, C., De Gouw, J. A., Maben, J. R., Wagner, N. L., Riedel, T. P.,
 1519 Thornton, J. A., Wolfe, D. E., Dubé, W. P., Öztürk, F., Brock, C. A., Grossberg, N., Lefer,
 1520 B., ... Roberts, J. M. (2013). Understanding the role of the ground surface in HONO
 1521 vertical structure: High resolution vertical profiles during NACHTT-11. *Journal of*

1522 *Geophysical Research Atmospheres*, 118(17), 10,155-10,171.
1523 <https://doi.org/10.1002/jgrd.50721>

1524 VandenBoer, T. C., Young, C. J., Talukdar, R. K., Markovic, M. Z., Brown, S. S., Roberts, J. M.,
1525 & Murphy, J. G. (2015). Nocturnal loss and daytime source of nitrous acid through reactive
1526 uptake and displacement. *Nature Geoscience*, 8(1), 55–60.
1527 <https://doi.org/10.1038/ngeo2298>

1528 Von Der Heyden, L., Wißdorf, W., Kurtenbach, R., & Kleffmann, J. (2022). A relaxed eddy
1529 accumulation (REA) LOPAP system for flux measurements of nitrous acid (HONO).
1530 *Atmospheric Measurement Techniques*, 15(6), 1983–2000. [https://doi.org/10.5194/amt-15-](https://doi.org/10.5194/amt-15-1983-2022)
1531 [1983-2022](https://doi.org/10.5194/amt-15-1983-2022)

1532 Wang, Fu, X., Wu, D., Wang, M., Lu, K., Mu, Y., Liu, Z., Zhang, Y., & Wang, T. (2021).
1533 Agricultural Fertilization Aggravates Air Pollution by Stimulating Soil Nitrous Acid
1534 Emissions at High Soil Moisture. *Environmental Science and Technology*, 55(21), 14556–
1535 14566. <https://doi.org/10.1021/acs.est.1c04134>

1536 Wang, Y., Fu, X., Wang, T., Ma, J., Gao, H., Wang, X., & Pu, W. (2022). Large Contribution of
1537 Nitrous Acid to Soil-Emitted Reactive Oxidized Nitrogen and Its Effect on Air Quality.
1538 *Environmental Science and Technology*. <https://doi.org/10.1021/acs.est.2c07793>

1539 Wolff, V., Trebs, I., Ammann, C., & Meixner, F. X. (2010). Atmospheric Measurement
1540 Techniques Aerodynamic gradient measurements of the NH₃-HNO₃-NH₄NO₃ triad using a
1541 wet chemical instrument: an analysis of precision requirements and flux errors. In *Atmos.*
1542 *Meas. Tech* (Vol. 3). www.atmos-meas-tech.net/3/187/2010/

1543 Wu, D., Deng, L., Liu, Y., Xi, D., Zou, H., Sha, Z., Pan, Y., Hou, L., & Liu, M. (2020).
1544 *Comparisons of the effects of different drying methods on soil nitrogen fractions: Insights*
1545 *into emissions of reactive nitrogen gases (HONO and NO)*.
1546 <https://doi.org/10.1080/16742834.2020.1733388>

1547 Wu, D., Horn, M. A., Behrendt, T., Müller, S., Li, J., Cole, J. A., Xie, B., Ju, X., Li, G., Ermel,
1548 M., Oswald, R., Fröhlich-Nowoisky, J., Hoor, P., Hu, C., Liu, M., Andreae, M. O., Pöschl,
1549 U., Cheng, Y., Su, H., ... Sörgel, M. (2019). Soil HONO emissions at high moisture content
1550 are driven by microbial nitrate reduction to nitrite: tackling the HONO puzzle. *ISME*
1551 *Journal*, 13(7), 1688–1699. <https://doi.org/10.1038/s41396-019-0379-y>

1552 Wu, D., Zhang, J., Wang, M., An, J., Wang, R., Haider, H., Xu-Ri, Huang, Y., Zhang, Q., Zhou,
1553 F., Tian, H., Zhang, X., Deng, L., Pan, Y., Chen, X., Yu, Y., Hu, C., Wang, R., Song, Y., ...
1554 Liu, M. (2022). Global and Regional Patterns of Soil Nitrous Acid Emissions and Their
1555 Acceleration of Rural Photochemical Reactions. *Journal of Geophysical Research:*
1556 *Atmospheres*, 127(6), 1–16. <https://doi.org/10.1029/2021JD036379>

1557 Yang, J. Y., Drury, C. F., Jiang, R., Worth, D. E., Bittman, S., Grant, B. B., & Smith, W. N.
1558 (2024). Reactive nitrogen losses from Canadian agricultural soils over 36 years. *Ecological*
1559 *Modelling*, 495. <https://doi.org/10.1016/j.ecolmodel.2024.110809>

1560 Young, C. J., Washenfelder, R. A., Roberts, J. M., Mielke, L. H., Ostho, H. D., Tsai, C.,
1561 Pikelnaya, O., Stutz, J., Veres, P. R., Cochran, A. K., Vandenboer, T. C., Flynn, J.,
1562 Grossberg, N., Haman, C. L., Lefer, B., Stark, H., Graus, M., Gouw, J. De, Gilman, J. B., ...
1563 Brown, S. S. (2012). *Vertically Resolved Measurements of Nighttime Radical Reservoirs in*
1564 *Los Angeles and Their Contribution to the Urban Radical Budget*.

1565 Zhang, S., Sarwar, G., Xing, J., Chu, B., Xue, C., Sarav, A., Ding, D., Zheng, H., Mu, Y., Duan,
1566 F., Ma, T., & He, H. (2021). Improving the representation of HONO chemistry in CMAQ
1567 and examining its impact on haze over China. *Atmospheric Chemistry and Physics*, *21*(20),
1568 15809–15826. <https://doi.org/10.5194/acp-21-15809-2021>

1569 Zhou, S., Young, C. J., VandenBoer, T. C., Kowal, S. F., & Kahan, T. F. (2018). Time-Resolved
1570 Measurements of Nitric Oxide, Nitrogen Dioxide, and Nitrous Acid in an Occupied New
1571 York Home. *Environmental Science and Technology*, *52*(15), 8355–8364.
1572 <https://doi.org/10.1021/acs.est.8b01792>

1573 Zörner, J., Penning De Vries, M., Beirle, S., Sihler, H., Veres, P. R., Williams, J., & Wagner, T.
1574 (2016). Multi-satellite sensor study on precipitation-induced emission pulses of NO_x from soils
1575 in semi-arid ecosystems. *Atmospheric Chemistry and Physics*, *16*(14), 9457–9487.
1576 <https://doi.org/10.5194/acp-16-9457-2016>